Czech Technical University in Prague
Faculty of Electrical Engineering
Department of Cybernetics

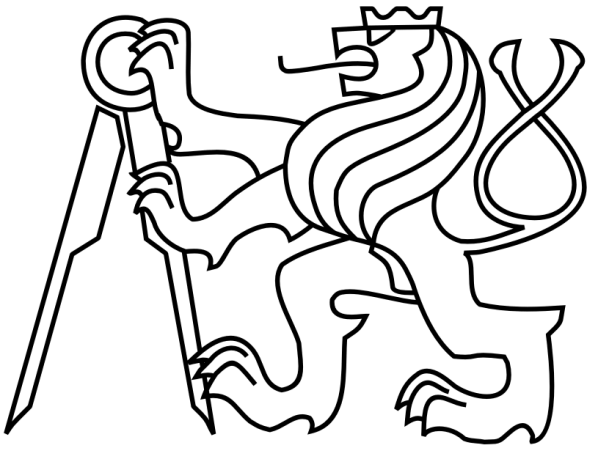

Bachelor Thesis

Single-Track Mobile Robot Control

Author: Jan Hauser

Supervisor: Ing. Jiří Dostál

Prague, May, 2014

Czech Technical University in Prague
Faculty of Electrical Engineering

Department of Cybernetics

BACHELOR PROJECT ASSIGNMENT

Student: Jan H a u s e r

Study programme: Cybernetics and Robotics

Specialisation: Robotics

Title of Bachelor Project: Single-Track Mobile Robot Control

Guidelines:

1. Construct a prototype of a single-track mobile robot from a LEGO Mindstorms kit.
2. Identify a dynamic model of the robot.
3. Develop and implement a controller for lateral stabilization of the robot.
4. Develop and implement a controller for the robot in forward motion.

Bibliography/Sources:

[1] K. J. Astrom, D. J. Block, and M. W. Spong: The Reaction Wheel Pendulum. Morgan & Claypool, 2007.
[2] Forbes T. Brown: Engineering system dynamics : a unified graph-centered approach. Boca Raton, FL: CRC Taylor & Francis, 2007.
[3] L. Ljung: System Identification: Theory for the User. Prentice Hall, 1987.
[4] P. J. Antsaklis and A. N. Michel: A Linear Systems Primer. Birkhauser, 2007.
[5] G. F. Franklin, J. D. Powell, and A. Emami-Naeini: Feedback Control of Dynamic Systems. Prentice Hall, 2005.

Bachelor Project Supervisor: Ing. Jiří Dostál

Valid until: the end of the summer semester of academic year 2014/2015

L.S.

doc. Dr. Ing. Jan Kybic
Head of Department

prof. Ing. Pavel Ripka, CSc.
Dean

Prague, December 16, 2013

České vysoké učení technické v Praze
Fakulta elektrotechnická

Katedra kybernetiky

ZADÁNÍ BAKALÁŘSKÉ PRÁCE

Student: Jan H a u s e r

Studijní program: Kybernetika a robotika (bakalářský)

Obor: Robotika

Název tématu: Řízení jednostopého mobilního robota

Pokyny pro vypracování:

1. Zkonstruujte prototyp jednostopého robota ze stavebnice LEGO Mindstorms.
2. Identifikujte dynamický model systému robota.
3. Navrhněte metodu laterální stabilizace robota a stabilizaci realizujte.
4. Navrhněte řízení jízdy robota a řízení realizujte.

Seznam odborné literatury:

[1] K. J. Astrom, D. J. Block, and M. W. Spong: The Reaction Wheel Pendulum. Morgan & Claypool, 2007.
[2] Forbes T. Brown: Engineering system dynamics : a unified graph-centered approach. Boca Raton, FL: CRC Taylor & Francis, 2007.
[3] L. Ljung: System Identification: Theory for the User. Prentice Hall, 1987.
[4] P. J. Antsaklis and A. N. Michel: A Linear Systems Primer. Birkhauser, 2007.
[5] G. F. Franklin, J. D. Powell, and A. Emami-Naeini: Feedback Control of Dynamic Systems. Prentice Hall, 2005.

Vedoucí bakalářské práce: Ing. Jiří Dostál

Platnost zadání: do konce letního semestru 2014/2015

L.S.

doc. Dr. Ing. Jan Kybic
vedoucí katedry

prof. Ing. Pavel Ripka, CSc.
děkan

V Praze dne 16. 12. 2013

Declaration/Prohlášení

I hereby formally declare that I worked out the presented thesis independently and I quoted all used resources (literature, projects, software etc.) in accord with Methodical instructions about ethical principles for writing academic thesis.

Prohlašuji, že jsem předloženou práci vypracoval samostatně a že jsem uvedl veškeré použité informační zdroje v souladu s Metodickým pokynem o dodržování etických principů při přípravě vysokoškolských závěrečných prací.

In Prague, date / V Praze dne: ..... Signature / Podpis: .....

Acknowledgement

Foremost, I would like to express my sincere thanks to my supervisor Ing. Jiří Dostál for his excellent guidance, improvement proposals and helpful comments.

I also want to give thanks to numberless open source developers who indirectly made implementation of all my software components possible by sharing code and thoughts with the general public.

Finally, my great gratitude goes to my family and classmates for their support and endless patience.

Abstract

The aim of this thesis is to stabilize a single-track mobile robot in a vertically upright position while the robot is in motion as well as while it is motionless.

This system is modeled using a MATLAB Simulink environment and applied to a real system built with a help of LEGO Mindstorms building kit.

In the first section of the thesis a lateral stabilizating model and a planar model of motion are described with all the derivations.

Further, the real system is presented with a description of a construction, an identification and the limitations linked with the LEGO Mindstorms building kit and the LEGO sensors. The comparison of the real and identified systems is also a necessary part of this section.

The final section is indicative of a real model control description and a real measured data presentation. The real measured data is realized on the built single-track mobile robot.

Aim of the thesis

1. Construct a prototype of a single-track mobile robot from a LEGO Minstorms kit.
2. Identify a dynamic model of the robot.
3. Develop and implement a controller for lateral stabilization of the robot.
4. Develop and implement a controller for the robot in forward motion.

Abstrakt

Tato práce se zabývá řízením jednostopého vozidla z hlediska laterální stabilizace v klidu i v pohybu.

Zaměřil jsem se předně na namodelování samotného systému v prostředí MATLAB Simulink a následně na aplikaci získaného modelu na reálný systém, který byl realizován s využitím sestavy LEGO Mindstorms.

V práci nejprve popisuji modelování z hlediska samostantné laterální stabilizace, následně je v první sekci přidán planární pohybový model.

Dále je představen reálný model, jeho konstrukce, identifikace a omezení, která s sebou přináší sestava LEGO Mindstorms s příslušnými senzory. Porovnání identifikovaného a reálného modelu je nezbytnou součástí této sekce.

Cílem poslední sekce této práce je popsat samotné řízení reálného modelu, představit naměřená reálná data realizovaná na skutečném modelu jednostopého vozidla.

Contents

List of Figures

Nomenclature

DC-motor

$\mathcal{L}$	Lagrangian	[-]
ω	angular velocity	$[^{rad}/_{s}]$
τ	motor torque	[Nm]
τ_z	total external load moment of force	[Nm]
φ	angle of arbor	[rad]
b	friction constant	$[^{kgm^2}/_{s}]$
i	current	[A]
J	moment of inertia	$[kgm^2]$
k_e	electric constant	$[^{V}/_{rad/s}]$
k_t	torque constant	$[^{Nm}/_{A}]$
L	inductance	[H]
R	resistance	[Ω]
T	kinetic energy	[J]
u	voltage	[V]
V	potential energy	[J]

Lateral Dynamics Model

ω_B	angular velocity of body	$[^{rad}/_{s}]$
ω_G	angular velocity of gyroscopic axis	$[^{rad}/_{s}]$
ω_W	angular velocity of reaction wheel	$[^{rad}/_{s}]$
τ	reaction wheel torque	[Nm]
τ_G	gyroscopic disc torque	[Nm]
φ_B	angle of body	[rad]
φ_G	angle of gyroscopic disc	[rad]
φ_W	angle of reaction wheel	[rad]
g	gravitational acceleration	$[^{m}/_{s^2}]$
J_B	moment of inertia of body about it's center of mass	$[kgm^2]$
J_W	moment of inertia of reaction wheel about it's center of mass	$[kgm^2]$
k_B	viscous friction of body	$[^{N}/_{m}]$
k_W	viscous friction of reaction wheel	$[^{N}/_{m}]$
l_1	distance from pivot to center of mass of body	[m]
l_2	distance between centers of mass of body and reaction wheel	[m]
m_B	mass of body	[kg]
m_W	mass of reaction wheel	[kg]

Planar Model of Motion

α	angle of front wheel	[rad]
$\ddot{\eta}$	yaw acceleration	$[^{m}/_{s^2}]$
$\dot{\eta}$	yaw rate	$[^{rad}/_{s}]$
η	yaw angle	[rad]
θ	angle of body	[rad]
a	distance between centers of wheels	[m]
$a_{\ddot{\eta}}$	yaw acceleration	$[^{rad}/_{s^2}]$
$a_{\dot{\eta}}$	normal acceleration toward center of turn	$[^{rad}/_{s^2}]$
$a_{\dot{\omega_B}}$	roll acceleration	$[^{rad}/_{s^2}]$
b	horizontal distance to center of mass	[m]
l	vertical distance to center of mass	[m]
m	mass of motorcycle	[kg]
R	distance to yaw center of rotation	[m]
v	forward velocity	$[^{m}/_{s}]$

1 Introduction

Every motorbike moving down the street obviously needs a driver who keeps it in the vertically upright position. The first motivation for this thesis was an idea of how to keep the motorbike in the upright position just by itself without the intervention of the driver. Few relatively actual researches deal with this issue.

Three methods of a lateral stabilization are published. The most frequent solution is a reaction wheel control. This method is published as an analogy in the form of a reaction wheel pendulum [10, 11, 12, 13], or in the applied form as the reaction wheel control of a selfbalancing motorbike [9]. A slightly different method is published in [15], but it is basically the same as the reaction wheel. The smoothest method is the lateral stabilization using a gyroscope. Gyroscopic stabilizer is presented in [14].

The first selected solution was the **reaction wheel pendulum** [1]. Taking into consideration all the simplifications, we can liken the single-track robot standing still to the reaction wheel pendulum. This type of pendulum is essentially an inverted pendulum with a rotary wheel attached on its free end. A more accurate description is shown in the first section of this thesis. The reaction wheel is able to stabilize the inverted pendulum, or the single-track robot in the position vertically up due to its dynamics. Some functional prototypes were already realized with satisfactory results, but never using the LEGO Mindstorms building kit and therefore this thesis was created.

The reaction wheel influences the pendulum with or without an external drive. A DC-motor or other types of drives are necessary to control a pendulum position using the reaction wheel. A laboratory model is presented in the Figure 1.

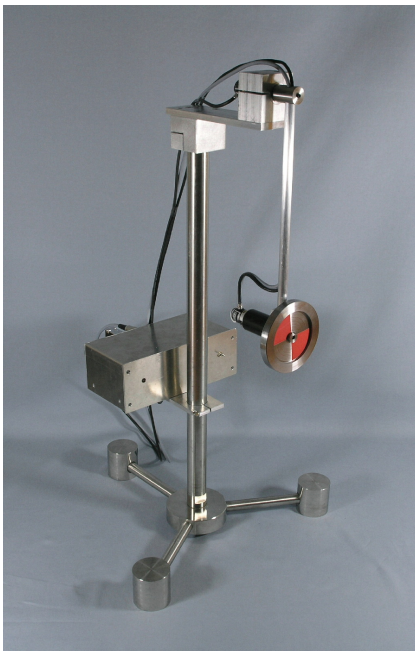

Figure 1: Laboratory model of the reaction wheel pendulum. Available from [16]

In the section 2.3, the detailed derivation of this model as well as the control derivation are shown.

This method was evaluated as the most feasible solution for the real model and was designed despite the LEGO construction limitations.

The **gyroscopic control** is presented as the second selected method. Main derivation of this method is made in the appendix A. The gyroscopic control is based on two-axis gimbal which are acctuated by a DC-motor and which balance the body of the single-track robot and prevent it from falling down using an interaction between the moments of force. The rotation axis of a gyroscope is generally perpendicular to the rotation axis of the robot. The gyroscope spins with a constant angular velocity and an influence to the robot's body is produced by changing a yaw velocity of gyroscope's rotation axis. This method proved to be very impressive. The C-1 model of the motorcycle with the gyroscopic control is able to use, its design is presented in the following Figure with appropriate link to manufacturer.

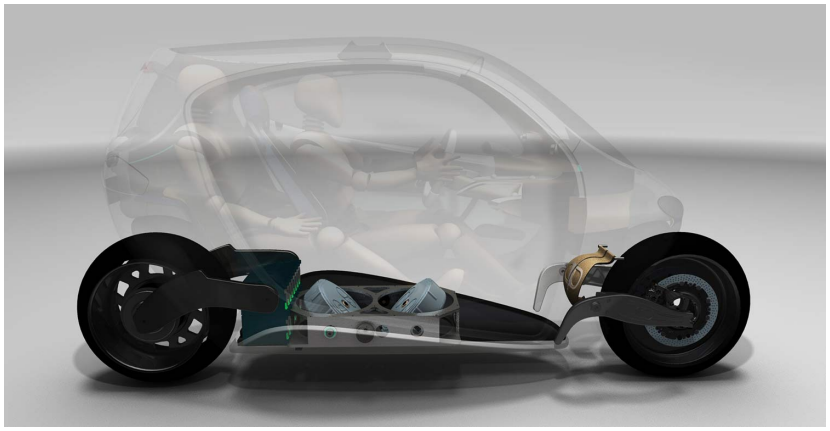

Figure 2: Real motorcycle controled by gyroscopic effect. Available from [18]

After a lateral stabilization it is necessary to set the model in motion. The planar model of motion described in the section 2.4 is really simple when the lateral stabilization is solved and the results are once again quite interesting, see the Figure 22a. The important fact is that a robot's handlebar is assumed to be actuated by a drive and therefore it cannot move freely. A free handlebar brings other difficulties which are not needed to be dealt with in this thesis.

Further, the thesis pursues the realization of a real model. The construction limitations are obvious, but the final construction is durable and quite good looking (Fig. 3). The identification usually goes before control and this thesis is no exception. Some interesting identification experiments are presented with satisfactory results. The control is derived and applied to the real model, it is all described in the section 4.

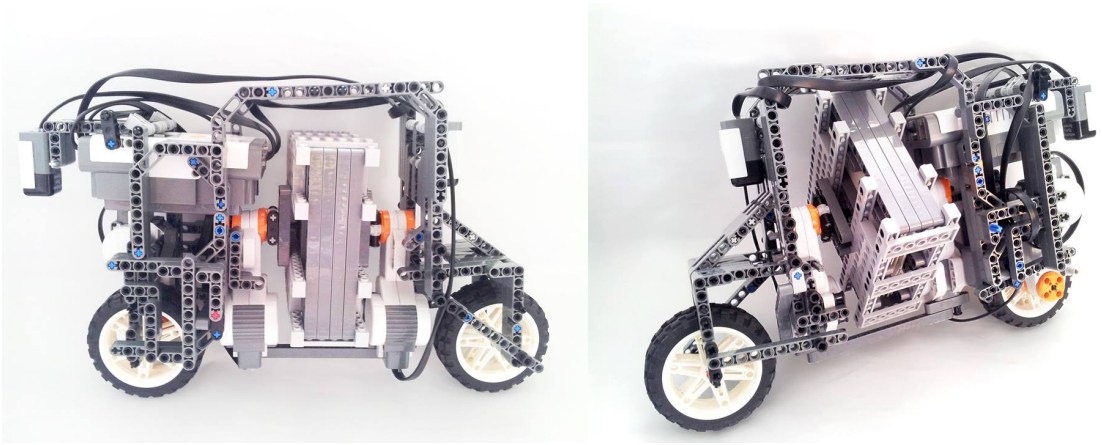

Figure 3: Single-track mobile robot constructed with a help of the LEGO Mindstorms building kit.

2 Model

The main problem of keeping the single-track mobile robot in an upright direction can be solved in several different ways. The reaction wheel control and the gyroscopic control were chosen during the analysis of single-track mobile robot lateral stabilization. The reaction wheel was selected as the most feasible method which could be applied to the real model and the gyroscopic control as the most interesting and elegant way to the single-track mobile robot lateral stabilization. Both methods and appropriate models are described in this section. A DC-motor is a drive in both methods and according to this fact its dynamics is described here.

2.1 DC-motor Dynamics

2.1.1 Equations of Motion

The dynamics of the DC-motor is described by these equations.

$$\begin{aligned} L\frac{di(t)}{dt} &= -Ri(t) - k_e\omega(t) + u(t) \\ J\frac{d\omega(t)}{dt} &= k_t i(t) - b\omega(t) - \tau_z(t) \\ \tau(t) &= k_t i(t) \end{aligned} \tag{1}$$

where the torque constant k_t is identical to the back EMF constant k_e in other units.

variable	***unit***	***description***
i	A	current
u	V	voltage
τ_z	Nm	total external load moment of force
ω	$^{\mathrm{rad}}/_{\mathrm{s}}$	angular velocity
φ	rad	angle of arbor
τ	Nm	motor torque
R	Ω	resistance
L	H	inductance
J	kgm^2	moment of inertia
b	$^{\mathrm{kgm}^2}/_{\mathrm{s}}$	friction constant
k_e	$^{\mathrm{V}}/_{\mathrm{rad/s}}$	electric constant
k_t	$^{\mathrm{Nm}}/_{\mathrm{A}}$	torque constant

Table 1: Used variables

2.1.2 State Space Model

One system simplification is possible because of uncomparatively fast time constant of motor current to the rest of the states.

$$\frac{di(t)}{dt} = 0$$

The state space model is defined according to the equations 2.

$$\begin{aligned} \dot{\boldsymbol{x}} &= \boldsymbol{A}\boldsymbol{x} + \boldsymbol{B}\boldsymbol{u} \\ \boldsymbol{y} &= \boldsymbol{C}\boldsymbol{x} + \boldsymbol{D}\boldsymbol{u} \end{aligned} \tag{2}$$

$$\begin{aligned} \begin{bmatrix} \frac{d\omega(t)}{dt} \\ \frac{d\varphi(t)}{dt} \end{bmatrix} &= \begin{bmatrix} -\frac{k_e k_m}{RJ} - b & 0 \\ 1 & 0 \end{bmatrix} \begin{bmatrix} \omega(t) \\ \varphi(t) \end{bmatrix} + \begin{bmatrix} \frac{k_m}{RJ} & -1 \\ 0 & 0 \end{bmatrix} \begin{bmatrix} u(t) \\ \tau_z(t) \end{bmatrix} \\ \tau &= \begin{bmatrix} -\frac{k_t k_e}{R} & 0 \end{bmatrix} \begin{bmatrix} \omega(t) \\ \varphi(t) \end{bmatrix} + \begin{bmatrix} \frac{k_t}{R} & 0 \end{bmatrix} \begin{bmatrix} u(t) \\ \tau_z(t) \end{bmatrix} \end{aligned} \tag{3}$$

All the types of LEGO motors are presented in [5]. The motor with the ideal combination of rotation speed and stalled torque is used in the construction. The NXT motor is chosen.

2.2 Lateral Dynamics Model with Reaction Wheel

The reaction wheel, sometimes also referred to as the momentum wheel, is a simple rotating wheel which is attached to the shaft of a DC-motor. The wheel is placed in the vertical axis of the robot. Mutual torque between the wheel and robot can be used to control the vertical position of the robot. The robot with the reaction wheel can be likened to the reaction wheel pendulum [1].

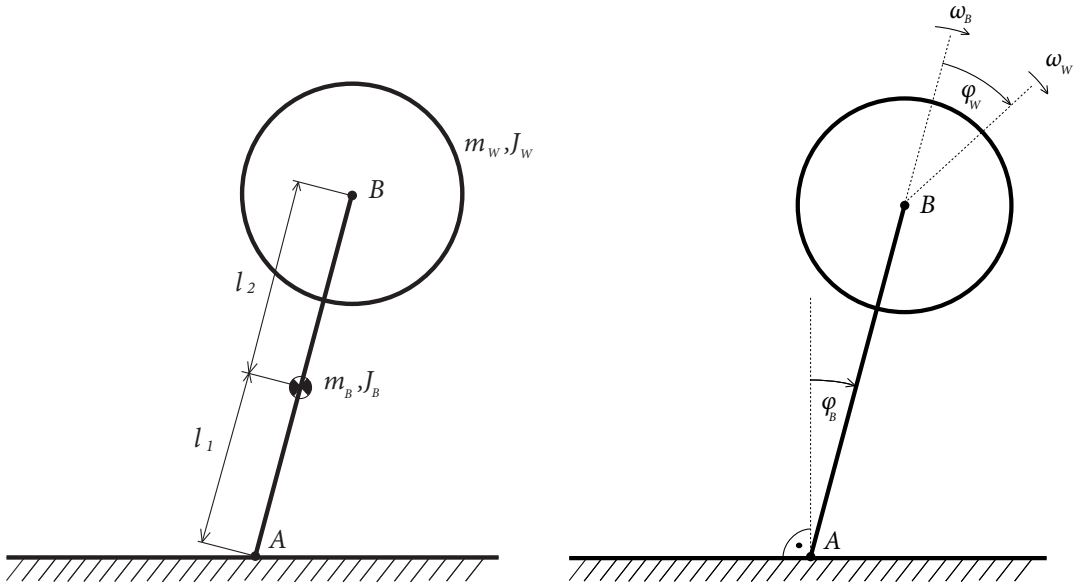

(a) Physical dimensions (b) State variables

Figure 4: The principle of single-track mobile robot lateral stabilization is described with the reaction wheel pendulum. The robot is standing still and balancing. The direction $|AB|$ marks the body of the robot and the circle with its center in B interpretes the reaction wheel.

The moment of force τ formed by the reaction wheel acts in the point B, but the influence on the body which is called "actuator moment" is in the point A with opposite sign.

All the variables shown in the Figure 4 are described in the following table.

variable	***unit***	***description***
m_B	kg	mass of body
m_W	kg	mass of reaction wheel
l_1	m	distance from pivot to center of mass of body
l_2	m	distance between centers of mass of body and reaction wheel
J_B	kgm^2	moment of inertia of body about it's center of mass
J_W	kgm^2	moment of inertia of reaction wheel about it's center of mass
φ_B	rad	angle of body
φ_W	rad	angle of reaction wheel
ω_B	$^{\mathrm{rad}}/_{\mathrm{s}}$	angular velocity of body
ω_W	$^{\mathrm{rad}}/_{\mathrm{s}}$	angular velocity of reaction wheel
τ	Nm	reaction wheel torque
k_B	$^{\mathrm{N}}/_{\mathrm{m}}$	viscous friction of body (in point A)
k_W	$^{\mathrm{N}}/_{\mathrm{m}}$	viscous friction of reaction wheel (in point B)

Table 2: Used variables

2.2.1 Equations of Motion

The equations of motion derivation preceded description of the system. The reaction wheel pendulum has one DOF. The relation for the distance to the wheel's axis is added here because of simplification.

$$l = l_1 + l_2$$

The body's moment of inertia with respect to the point A is defined using the Huygens–Steiner theorem.

$$J_B = J_W + m_B l_1^2 + m_W l^2 \tag{4}$$

The kinetic energy $T\,[J]$ and the potential energy $V\,[J]$ are defined

$$\begin{aligned} T &= \frac{1}{2} J_B \omega_B^2 + \frac{1}{2} J_W \omega_W^2 \\ V &= g \cos(\varphi_B)\,(m_B l_1 + m_W l) \end{aligned}$$

2.2.1.1 Equations of Motion without Friction

The equations of motion are determined using the Lagrange's method.

$$\frac{d}{dt}\left(\frac{\partial \mathcal{L}}{\partial \dot{\boldsymbol{q}}}\right) + \frac{\partial \mathcal{L}}{\partial \boldsymbol{q}} = 0 \tag{5}$$

First step is to define the Lagrangian function $\mathcal{L}$ and the generalized coordinates and velocities, $\boldsymbol{q}$, $\dot{\boldsymbol{q}}$.

$$\mathcal{L} = T - V$$

$$\begin{aligned} \boldsymbol{q} &= \begin{bmatrix} \varphi_B \\ \varphi_W \end{bmatrix} \\ \dot{\boldsymbol{q}} &= \begin{bmatrix} \omega_B \\ \omega_W \end{bmatrix} \end{aligned} \tag{6}$$

After differentiation

$$\begin{aligned} \frac{d}{dt}\left(\frac{\partial \mathcal{L}}{\partial \dot{\boldsymbol{q}}}\right) &= \begin{bmatrix} J_B \dot{\omega_B} \\ J_W \dot{\omega_W} \end{bmatrix} \\ \frac{\partial \mathcal{L}}{\partial \boldsymbol{q}} &= \begin{bmatrix} -g \sin(\varphi_B)\,(m_B l_1 + m_W l) \\ 0 \end{bmatrix} \end{aligned} \tag{7}$$

The basic equations of motion of the reaction wheel pendulum are derived.

$$\begin{aligned} \dot{\omega_B} - \frac{g \cdot (m_B l_1 + m_W l)}{J_B} \sin(\varphi_B) &= 0 \\ J_W \dot{\omega_W} &= 0 \end{aligned} \tag{8}$$

Note that the friction and other interaction are neglected in this chapter.

2.2.1.2 Equations of Motion with Friction

Some modifications had to be carried out in order to make the theoretical model more realistic. All the frictions and interactions between the body and the reaction wheel are neglected in the previous section. That includes mainly the friction at points A and B (Fig. 4). The final state equations are determined.

$$\begin{aligned} \dot{\omega}_B &= \frac{1}{J_B} \left[g \sin(\varphi_B) (m_B l_1 + m_W l) - \tau + k_W \omega_W - (k_W + k_B) \omega_B \right] \\ \dot{\omega}_W &= \frac{1}{J_W} \left[\tau - k_W (\omega_W - \omega_B) \right] \\ \dot{\varphi}_B &= \omega_B \end{aligned} \tag{9}$$

These state equations contain all the frictions, interactions and torque from the reaction wheel.

2.2.2 State Space Model

It is important to define all the states, inputs and outputs. This state space model has only one input, the moment of force τ and only one state to observe as the output, the angle of body φ_B. One simplification is also applied to the model, the angle of wheel φ_W is neglected because of its irrelevance. The state vectors of the system are

$$\begin{aligned} \boldsymbol{x}(t) &= \begin{bmatrix} \omega_B(t) & \varphi_B(t) & \omega_W(t) \end{bmatrix}^T \\ u(t) &= \tau(t) \\ y(t) &= \varphi_B(t) \end{aligned} \tag{10}$$

Here it is also defined that all the variables and states are variable in time. This fact is not going to be highlighted any more in this thesis.

The equations 9 could be now rewritten to matrix representation.

$$\begin{aligned} \dot{\boldsymbol{x}} &= \boldsymbol{A}\boldsymbol{x} + \boldsymbol{B}\boldsymbol{u} + h(\boldsymbol{x}, \boldsymbol{u}) \\ \boldsymbol{y} &= \boldsymbol{C}\boldsymbol{x} + \boldsymbol{D}\boldsymbol{u} \end{aligned} \tag{11}$$

$$\begin{aligned} \dot{\boldsymbol{x}} &= \begin{bmatrix} -\frac{k_B+k_W}{J_B} & 0 & \frac{k_W}{J_B} \\ 1 & 0 & 0 \\ \frac{k_W}{J_W} & 0 & -\frac{k_W}{J_W} \end{bmatrix} \boldsymbol{x} + \begin{bmatrix} -\frac{1}{J_B} \\ 0 \\ \frac{1}{J_W} \end{bmatrix} u + \begin{bmatrix} \frac{g\sin(\varphi_B)(m_B l_1 + m_W l)}{J_B} \\ 0 \\ 0 \end{bmatrix} \\ y &= \begin{bmatrix} 0 & 1 & 0 \end{bmatrix} \boldsymbol{x} \end{aligned} \tag{12}$$

This state space model is nonlinear because of the first equation describing the variable ω_B. The linearization has to be made in a suitable stationary point called the equilibrium.

2.2.2.1 Linearization

First of all, the ideal equilibrium has to be found. All the possibilities of the equilibrium are given by the equation

$$\dot{\boldsymbol{x}} = 0 \tag{13}$$

For the input operation point

$$u_\varepsilon = 0$$

the solutions of equation 13 are

$$\begin{aligned} \boldsymbol{x}_{\boldsymbol{\varepsilon_1}} &= \begin{bmatrix} 0 & 0 & 0 \end{bmatrix}^T \\ \boldsymbol{x}_{\boldsymbol{\varepsilon_2}} &= \begin{bmatrix} 0 & \pi & 0 \end{bmatrix}^T \end{aligned} \tag{14}$$

The main intention is to hold the body of the model in the vertically up position, therefore upper equilibrium $\boldsymbol{x}_{\boldsymbol{\varepsilon_1}}$ is taken as the equilibrium.

$$\boldsymbol{x}_{\boldsymbol{\varepsilon}} = \boldsymbol{x}_{\boldsymbol{\varepsilon_1}}$$

Rewriting the first equation as

$$\dot{x_1} = f_1(\boldsymbol{x}, u) \tag{15}$$

using the Taylor series and neglecting the quadratic and higher degrees, the linearized deviation model is defined as

$$\dot{x_1} = f_1|_{\boldsymbol{x}=\boldsymbol{x}_{\boldsymbol{\varepsilon}}} + \left[\frac{\partial f_1}{\partial x_i}\right]\Big|_{\boldsymbol{x}=\boldsymbol{x}_{\boldsymbol{\varepsilon}}} \Delta\boldsymbol{x} + \left[\frac{\partial f_1}{\partial u}\right]\Big|_{\boldsymbol{x}=\boldsymbol{x}_{\boldsymbol{\varepsilon}}} \Delta u \tag{16}$$

Where $i = 1...n$ and n is the number of states. The deviation symbol Δ in front of the vectors is not necessary to write because of the zero operation point.

$$\begin{aligned} \Delta \boldsymbol{x} &= \boldsymbol{x} - \boldsymbol{x_\varepsilon} = \boldsymbol{x} \\ \Delta u &= u - u_\varepsilon = u \end{aligned}$$

The final linearized equation is determined as follows.

$$\dot{x_1} = \begin{bmatrix} -\frac{k_B+k_W}{J_B} & \frac{g(m_B l_1 + m_W l)}{J_B} & \frac{k_W}{J_B} \end{bmatrix} \boldsymbol{x} + \begin{bmatrix} -\frac{1}{J_B} \end{bmatrix} u \tag{17}$$

2.2.2.2 Linearized State Space Model

The linearization in equlibrum $\boldsymbol{x_\varepsilon}$ is successfully done and now the linearized state space model is possible to make according to the general state space equations 2. The state vectors are defined in the equations 10 and the matrices of system are determined as follows

$$\boldsymbol{A} = \begin{bmatrix} -\frac{k_B+k_W}{J_B} & \frac{g(m_B l_1 + m_W l)}{J_B} & \frac{k_W}{J_B} \\ 1 & 0 & 0 \\ \frac{k_W}{J_W} & 0 & -\frac{k_W}{J_W} \end{bmatrix} \boldsymbol{B} = \begin{bmatrix} -\frac{1}{J_B} \\ 0 \\ \frac{1}{J_W} \end{bmatrix} \tag{18}$$

$$\boldsymbol{C} = \begin{bmatrix} 0 & 1 & 0 \end{bmatrix} \; D = 0$$

Applying to equations 2.

$$\begin{aligned} \dot{\boldsymbol{x}} &= \begin{bmatrix} -\frac{k_B+k_W}{J_B} & \frac{g(m_B l_1 + m_W l)}{J_B} & \frac{k_W}{J_B} \\ 1 & 0 & 0 \\ \frac{k_W}{J_W} & 0 & -\frac{k_W}{J_W} \end{bmatrix} \boldsymbol{x} + \begin{bmatrix} -\frac{1}{J_B} \\ 0 \\ \frac{1}{J_W} \end{bmatrix} u \\ y &= \begin{bmatrix} 0 & 1 & 0 \end{bmatrix} \boldsymbol{x} \end{aligned} \tag{19}$$

This is the linearized state space model of reaction wheel pendulum valid around the equilibrium $\boldsymbol{x_\varepsilon}$.

2.2.3 Reaction Wheel Position Analysis

The distance of the reaction wheel from the body's center of gravity is determined as the most important parameter. The ideal position was found right in or below the center of gravity because of the lower value of input τ or the smaller maximal speed of reaction wheel ω_W.

The infuence of the reaction wheel position with respect to the body´s center of gravity is presented in the Figure 5.

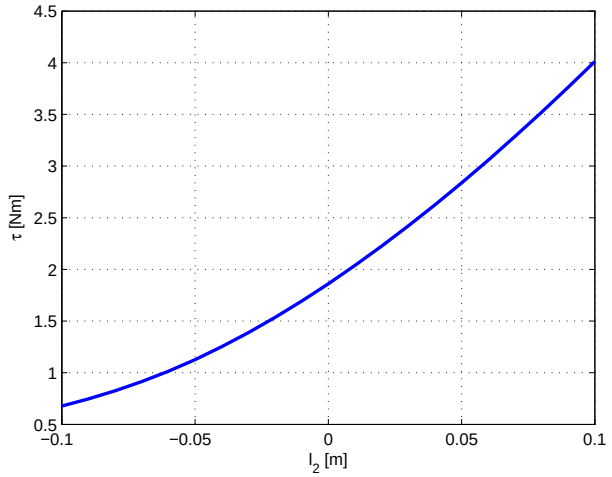

Figure 5: Initial torque peak needed for stabilization from constant nonzero tilt angle $\varphi_B(0) = 0.1745\,\text{rad}$ related to the reaction wheel distance from the center of gravity of the robot.

The position with the smallest value of l_2 is theoretically the ideal position of the reaction wheel because of decreasing requirements on the torque τ. This is in fact not possible to accomplish on the real model. This fact is considered during the construction and the reaction wheel is settled to the robot's center of gravity to the lowest possible position.

2.3 Lateral Dynamics Model with Gyroscope

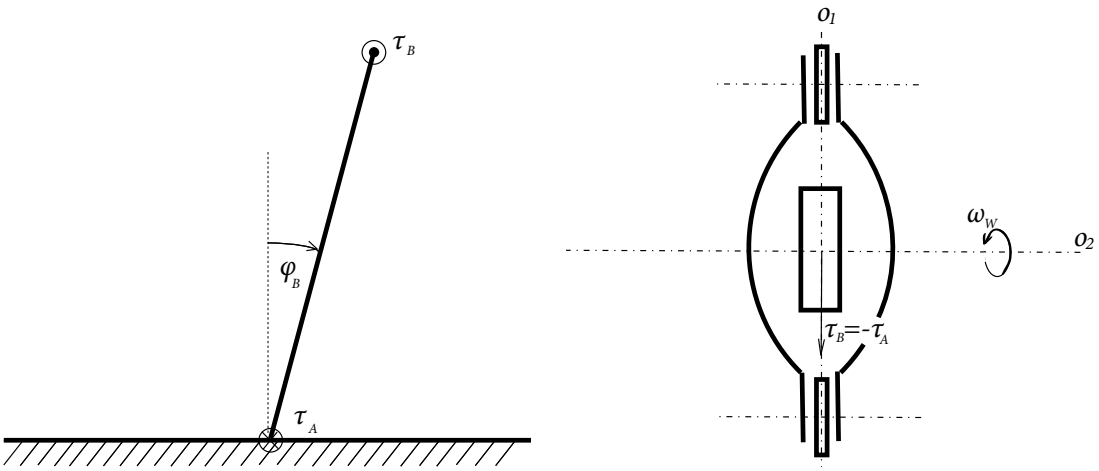

(a) Actuator moment τ_A and moment of force produced by gyro τ_B with relation $\tau_B = -\tau_A$.

(b) Position of gyroscopic actuator with description of moments direction.

Figure 6: Description of gyroscopic effect where ω_W is the constant angular velocity of gyrowheel ensuring the lateral stabilization and producing the actuator moment τ_B.

Model of the single-track mobile robot controlled by the gyroscopic effect is shown in the Figures 6, 7. A disc in the middle of the robot's body is represented by the rectangle. The moment of force τ_B

produced by the disc influences the body as the moment of force τ_A.

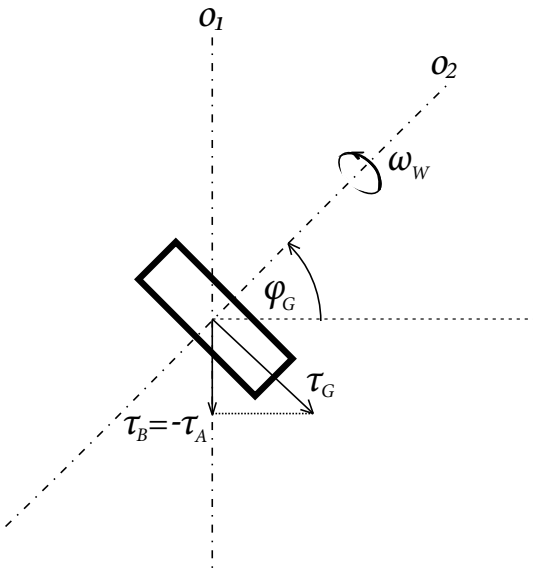

Figure 7: Description of gyroscopic effect with the rotation of gyrowheel by the angle φ_G. The moment of force τ_G is the torque produced by gyrowheel, the moment τ_B, or $-\tau_A$ is the actuator torque.

2.3.1 Equations of Motion

The equation 63 is rewritten for the purposes of this thesis according to the Figures 6, 7.

$$\begin{aligned} \tau_B &= J_W \omega_G \omega_W \\ \tau_A &= -\tau_B cos\left(\varphi_G\right) \end{aligned} \tag{20}$$

Body dynamics substituted by an inverted pendulum is the same as in the section 2.2, it is not necessary to rewrite these equations again.

Detailed derivation of gyroscopic effect is given in the appendix A.

2.3.1.1 Equations of Motion with Friction

The state equations are determined by assuming only the friction of the body.

$$\begin{aligned} \dot{\omega_B} &= \frac{1}{J_B}\left[-J_W \omega_G \omega_W \cos\left(\varphi_G\right) + g \sin\left(\varphi_B\right)\left(m_B l_1 + m_W l\right) - k_B \omega_B\right] \\ \dot{\omega_W} &= 0 \\ \dot{\varphi_B} &= \omega_B \\ \dot{\varphi_G} &= \omega_G \end{aligned} \tag{21}$$

2.3.2 State Space Model

A mathematical model of the single-track mobile robot gyroscopic control is defined according to the equations 21.

$$\begin{aligned} \boldsymbol{x} &= \begin{bmatrix} \omega_B & \varphi_B & \varphi_G \end{bmatrix}^T \\ u &= \omega_G \\ y &= \varphi_B \end{aligned} \tag{22}$$

The variable $\dot{\omega_W} = 0$, because ω_W is kept constant. It is not a state. Considering previous fact only the variable ω_G is able to change the rate of the moment of force , τ_B or τ_A as shown in the equation 20.

The nonlinear state space model is defined using the matrix description (eq. 11).

$$\begin{aligned} \dot{\boldsymbol{x}} &= \begin{bmatrix} -\frac{k_B}{J_B} & 0 & 0 \\ 1 & 0 & 0 \\ 0 & 0 & 0 \end{bmatrix} \boldsymbol{x} + \begin{bmatrix} 0 \\ 0 \\ 1 \end{bmatrix} u + \begin{bmatrix} -\frac{J_W \omega_W \omega_G \cos(\varphi_G)}{J_B} + \frac{g \sin(\varphi_B)(m_B l_1 + m_W l)}{J_B} \\ 0 \\ 0 \end{bmatrix} \\ y &= \begin{bmatrix} 0 & 1 & 0 \end{bmatrix} \boldsymbol{x} \end{aligned} \tag{23}$$

2.3.2.1 Linearization

The equilibrium is chosen as follows.

$$\boldsymbol{x_\varepsilon} = \begin{bmatrix} 0 & 0 & 0 \end{bmatrix}^T$$

The linearized deviation model is derived according to section 2.2.2.1.

$$\dot{x_1} = \begin{bmatrix} -\frac{k_B}{J_B} & \frac{g(m_B l_1 + m_W l)}{J_B} & 0 \end{bmatrix} \boldsymbol{x} + \begin{bmatrix} -\frac{J_W \omega_W}{J_B} \end{bmatrix} u \tag{24}$$

2.3.2.2 Linearized State Space Model

The linearized state space model and the state vectors are defined in this section pursuant to the equations 2. The state vectors:

$$\boldsymbol{A} = \begin{bmatrix} -\frac{k_B}{J_B} & \frac{g(m_B l_1 + m_W l)}{J_B} & 0 \\ 1 & 0 & 0 \\ 0 & 0 & 0 \end{bmatrix} \boldsymbol{B} = \begin{bmatrix} -\frac{J_W \omega_W}{J_B} \\ 0 \\ 1 \end{bmatrix}$$

$$\boldsymbol{C} = \begin{bmatrix} 0 & 1 & 0 \end{bmatrix} \; D = 0$$

The linearized state space model in the equilibrium $\boldsymbol{x_\varepsilon} = \begin{bmatrix} 0 & 0 & 0 \end{bmatrix}^T$:

$$\begin{aligned} \dot{\boldsymbol{x}} &= \begin{bmatrix} -\frac{k_B}{J_B} & \frac{g(m_B l_1 + m_W l)}{J_B} & 0 \\ 1 & 0 & 0 \\ 0 & 0 & 0 \end{bmatrix} \boldsymbol{x} + \begin{bmatrix} -\frac{J_W \omega_W}{J_B} \\ 0 \\ 1 \end{bmatrix} u \\ y &= \begin{bmatrix} 0 & 1 & 0 \end{bmatrix} \boldsymbol{x} \end{aligned} \tag{25}$$

2.4 Planar Model of Motion

After derivation of the lateral stabilization it is necessary to take a look at the factor of motion. The single-track mobile robot is set in motion by actuating of the rear wheel. The motion and rotation of the front wheel influences the lateral stabilization quite a lot. It also should be realized that when the robot moves into the curve, his vertical axis is inclined as shown in the final figure of this section. The planar model of motion using the reaction wheel for lateral stabilization is determined here according to [17]. The planar model of position is not omitted as well.

2.4.1 Equations of Motion

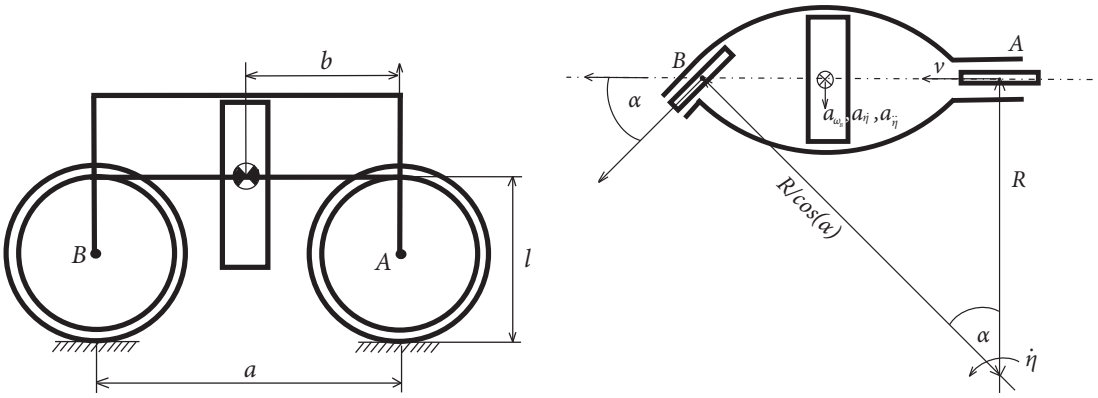

(a) Side view at the single-track mobile robot with defined important distances a, b, l. Rectangle in the middle represents the reaction wheel.

(b) View from above at the single-track mobile robot with defined front wheel rotation α and effects to body a_{ω_B}, $a_{\dot{\eta}}$, $a_{\ddot{\eta}}$, R represents necessary distance to define yaw rate $\dot{\eta}$.

Figure 8: Single-track mobile robot geometry with all defined parameters and demonstration of arrangement.

New parameters have to be defined to derivate the motion model. The description of these parameters can be found in the following table.

variable	***unit***	***description***
a	m	distance between centers of wheels
b	m	horizontal distance to center of mass
l	m	vertical distance to center of mass
R	m	distance to yaw center of rotation
m	kg	mass of motorcycle
v	$^{\mathrm{m}}/_{\mathrm{s}}$	forward velocity
α	rad	angle of front wheel
η	rad	yaw angle
$\dot{\eta}$	$^{\mathrm{rad}}/_{\mathrm{s}}$	yaw rate
$\ddot{\eta}$	$^{\mathrm{rad}}/_{\mathrm{s}^2}$	yaw acceleration
$a_{\dot{\omega_B}}$	$^{\mathrm{rad}}/_{\mathrm{s}^2}$	roll acceleration
$a_{\dot{\eta}}$	$^{\mathrm{rad}}/_{\mathrm{s}^2}$	normal acceleration toward center of turn
$a_{\ddot{\eta}}$	$^{\mathrm{rad}}/_{\mathrm{s}^2}$	yaw acceleration

Table 3: Used variables

The motion model geometry is shown in the Figure 8. There are two views in the Figure 8, the side view and the view from above. Rotation around the center of mass is described by the yaw angle η. The yaw rate and yaw acceleration directly relate to the yaw angle. The yaw rate is defined by the velocity v and the distance R.

$$\dot{\eta} = \frac{v}{R}$$

The parameter a is defined as the distance between the points A, B, where these points are located in the middle of wheels. Using the Pythagoras Theorem and the approximation for small angles, where $\cos(\alpha) = 1$ and $\sin(\alpha) = \alpha$, is defined

$$a = R\cos(\alpha)\sin(\alpha) \approx R\alpha$$

$$R = \frac{a}{\alpha}$$

The parameters $a_{\dot{\omega_B}} a_{\dot{\eta}}, a_{\ddot{\eta}}$ are conclusively dependent on the size of $\omega_B, \dot{\eta}, \ddot{\eta}$ changes. The normal acceleration $a_{\dot{\eta}}$ will exist even if the yaw rate $\dot{\eta}$ is constant and the motorcycle is travelling in a circular path, this acceleration is associated with the direction change of velocity. The accelerations $a_{\dot{\omega_B}}, a_{\ddot{\eta}}$ are the tangencial accelerations associated with φ_B and η. The values of accelerations are following

$$a_{\dot{\omega_B}} = l\dot{\omega}_B$$

$$a_{\dot{\eta}} = \frac{v^2}{R}$$

$$a_{\ddot{\eta}} = b\ddot{\eta}$$

Applying the Newton's Second Law of Motion

$$mgl\sin(\varphi_B) = ma_{\dot{\omega_B}}l + ma_{\dot{\eta}}\cos(\varphi_B)\,l + ma_{\ddot{\eta}}l + J_B\dot{\omega_B} \tag{26}$$

After substitutions

$$\dot{\omega_B}\left(l + \frac{J_B}{ml}\right) = g\sin(\varphi_B) - \frac{v^2}{R}\cos(\varphi_B) - b\ddot{\eta}$$

Using the relationship (v is defined as constant velocity)

$$\ddot{\eta} = \frac{d}{dt}\left(\frac{v}{R}\right) = \frac{d}{dt}\left(\frac{v\alpha}{a}\right) = \frac{v}{a}\dot{\alpha}$$

The final equation of motion is defined

$$\dot{\omega_B}\left(l + \frac{J_B}{ml}\right) = g\sin(\varphi_B) - \frac{v^2}{a}\cos(\varphi_B)\,\alpha - \frac{bv}{a}\dot{\alpha} \tag{27}$$

2.4.1.1 State Equations

The next step in the derivation process is the combination of equation 9 with the model defined in the section 2.2. The move effect has to be included only in the first state equation from the section 2, which is rewritten there

$$\dot{\omega_B} = \frac{1}{J_B}\left[g\sin(\varphi_B)\,(m_B l_1 + m_W l) - \tau + k_W\omega_W - (k_W + k_B)\,\omega_B\right] \tag{28}$$

The other equations are the same. The state equations of the motion model controlled by the reaction wheel are following

$$\begin{aligned}
\dot{\omega_B} &= \frac{1}{J_B}\left[(m_B l_1 + m_W l)\left(g\sin(\varphi_B) - \frac{v^2}{a}\cos(\varphi_B)\,\alpha - \frac{bv}{a}\dot{\alpha}\right) - \tau + k_W\omega_W - (k_W + k_B)\,\omega_B\right] + \\
&\quad + \frac{1}{l}\left(g\sin(\varphi_B) - \frac{v^2}{a}\cos(\varphi_B)\,\alpha - \frac{bv}{a}\dot{\alpha}\right) \\
\dot{\omega_W} &= \frac{1}{J_W}\left[\tau - k_W\,(\omega_W - \omega_B)\right] \\
\dot{\varphi_B} &= \omega_B
\end{aligned} \tag{29}$$

2.4.2 State Space Model

According to the state equations 29 the nonlinear state space model in the matrix description 11 is determined

$$\begin{aligned} \boldsymbol{x} &= \begin{bmatrix} \omega_B & \varphi_B & \omega_W & \alpha \end{bmatrix}^T \\ \boldsymbol{u} &= \begin{bmatrix} \tau & \dot{\alpha} \end{bmatrix}^T \\ y &= \varphi_B \end{aligned} \tag{30}$$

$$\begin{aligned} \dot{\boldsymbol{x}} &= \begin{bmatrix} -\frac{k_B+k_W}{J_B} & 0 & \frac{k_W}{J_B} & 0 \\ 1 & 0 & 0 & 0 \\ \frac{k_W}{J_W} & 0 & -\frac{k_W}{J_W} & 0 \\ 0 & 0 & 0 & 0 \end{bmatrix} \boldsymbol{x} + \begin{bmatrix} -\frac{1}{J_B} & \left(\frac{1}{l}+\frac{(m_B l_1+m_W l)}{J_B}\right)\left(-\frac{bv}{a}\right) \\ 0 & 0 \\ \frac{1}{J_W} & 0 \\ 0 & 1 \end{bmatrix} u + \\ &+ \begin{bmatrix} \frac{1}{J_B}\left[(m_B l_1 + m_W l)\left(g\sin(\varphi_B) - \frac{v^2}{a}\cos(\varphi_B)\,\alpha\right)\right] + \frac{1}{l}\left(g\sin(\varphi_B) - \frac{v^2}{a}\cos(\varphi_B)\,\alpha\right) \\ 0 \\ 0 \\ 0 \end{bmatrix} \\ y &= \begin{bmatrix} 0 & 1 & 0 & 0 \end{bmatrix} \boldsymbol{x} \end{aligned} \tag{31}$$

2.4.2.1 Linearization

Linearization is realized in the following equilibrium

$$\boldsymbol{x_\varepsilon} = \begin{bmatrix} 0 & 0 & 0 & 0 \end{bmatrix}^T$$

The linearized deviation motion model controlled by the reaction wheel is derived according to the section 2.2.2.1.

$$\begin{aligned} \dot{x_1} &= \begin{bmatrix} -\frac{k_B+k_W}{J_B} & \left(\frac{1}{l}+\frac{(m_B l_1+m_W l)}{J_B}\right) g & \frac{k_W}{J_B} & \left(\frac{1}{l}+\frac{(m_B l_1+m_W l)}{J_B}\right)\left(-\frac{v^2}{a}\right) \end{bmatrix} \boldsymbol{x} + \\ &+ \begin{bmatrix} -\frac{1}{J_B} & \left(\frac{1}{l}+\frac{(m_B l_1+m_W l)}{J_B}\right)\left(-\frac{bv}{a}\right) \end{bmatrix} u \end{aligned} \tag{32}$$

2.4.2.2 Linearized State Space Model

The definition of the state vectors

$$\begin{aligned} \boldsymbol{A} &= \begin{bmatrix} -\frac{k_B+k_W}{J_B} & \left(\frac{1}{l}+\frac{(m_B l_1+m_W l)}{J_B}\right) g & \frac{k_W}{J_B} & \left(\frac{1}{l}+\frac{(m_B l_1+m_W l)}{J_B}\right)\left(-\frac{v^2}{a}\right) \\ 1 & 0 & 0 & 0 \\ \frac{k_W}{J_W} & 0 & -\frac{k_W}{J_W} & 0 \\ 0 & 0 & 0 & 0 \end{bmatrix} \\ \boldsymbol{B} &= \begin{bmatrix} -\frac{1}{J_B} & \left(\frac{1}{l}+\frac{(m_B l_1+m_W l)}{J_B}\right)\left(-\frac{bv}{a}\right) \\ 0 & 0 \\ \frac{1}{J_W} & 0 \\ 0 & 1 \end{bmatrix} \end{aligned} \tag{33}$$

$$\boldsymbol{C} = \begin{bmatrix} 0 & 1 & 0 & 0 \end{bmatrix} \; D = 0$$

The definition of the final linearized state space model is also necessary

$$\begin{aligned} \dot{\boldsymbol{x}} &= \begin{bmatrix} -\frac{k_B+k_W}{J_B} & \left(\frac{1}{l}+\frac{(m_B l_1+m_W l)}{J_B}\right) g & \frac{k_W}{J_B} & \left(\frac{1}{l}+\frac{(m_B l_1+m_W l)}{J_B}\right)\left(-\frac{v^2}{a}\right) \\ 1 & 0 & 0 & 0 \\ \frac{k_W}{J_W} & 0 & -\frac{k_W}{J_W} & 0 \\ 0 & 0 & 0 & 0 \end{bmatrix} \boldsymbol{x} + \\ &+ \begin{bmatrix} -\frac{1}{J_B} & \left(\frac{1}{l}+\frac{(m_B l_1+m_W l)}{J_B}\right)\left(-\frac{bv}{a}\right) \\ 0 & 0 \\ \frac{1}{J_W} & 0 \\ 0 & 1 \end{bmatrix} u \\ y &= \begin{bmatrix} 0 & 1 & 0 & 0 \end{bmatrix} \boldsymbol{x} \end{aligned} \tag{34}$$

Position of the robot in the space with the body's angle of rotation is defined by these three equations

$$\begin{aligned} \dot{x} &= v\cos(\theta) \\ \dot{y} &= v\sin(\theta) \\ \dot{\theta} &= \frac{v}{l}\tan(\alpha) \end{aligned} \tag{35}$$

where x, y are the coordinates with their velocities $\dot{x}$, $\dot{y}$ and θ, $\dot{\theta}$ describes the directional rotation and velocity of the body.

3 Identification

The design of the real model is described in this chapter, it contains a description of construction, identification methods and also the limitations. The comparative simulations of real and identified models are presented at the end of this chapter. All the derived parameters are shown in the table below.

3.1 Robot's body

The real model of the single-track robot is realized with a help of the LEGO Mindstorms building kit. Due to the simplicity of mechanical setup, the reaction wheel was used in the real model as a stabilizing actuator.

The care is given primarly to the vertical axial symetry in the real model design. The moment of force of reaction wheel is dependent on the wheel's mass, it is not possible to construct the sufficiently heavy reaction wheel only with the LEGO components. According to this fact the load from an external source has to be used. The reaction wheel position is located directly in the middle of the robot's body and disturbs the structural strength of the robot. This problem is solved by fixing the front and rear parts of the body in the places above and below the reaction wheel.

Two LEGO NXT Motors are used to the actuation with the reaction wheel and it also contributes to the total strength of the real model. The construction also contains two gyroscopic sensors, the LEGO NXT Intelligent Brick and one LEGO NXT Motor for the rear-wheel drive.

The final costruction of the single-track robot is presented in the pictures below.

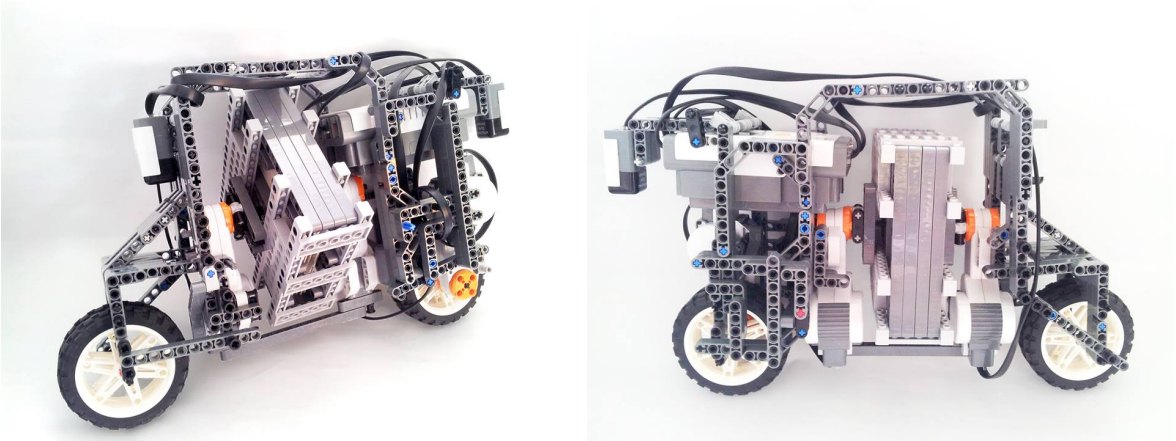

Figure 9: Real model of the single-track mobile robot made with a help of the LEGO Mindstorms building kit.

3.1.1 System Parameters

The equations 9 are rewriten here to demonstrate the unkown parameters. These parameters are bold in the equation 36. The other parameters are known, or rather directly or indirectly measured by the robot´s sensors. The simplification $(m_B l_1 + m_W l) \cong (m_B + m_W)\, l$ was applied as well.

$$\begin{aligned} \dot{\omega}_B &= \frac{1}{\boldsymbol{J_B}} \left[g \sin\left(\varphi_B\right) \left(\boldsymbol{m_B} + \boldsymbol{m_W} \right) \boldsymbol{l} - \tau + \boldsymbol{k_W} \omega_W - \left(\boldsymbol{k_W} + \boldsymbol{k_B} \right) \omega_B \right] \\ \dot{\omega}_W &= \frac{1}{\boldsymbol{J_W}} \left[\tau - \boldsymbol{k_W} \left(\omega_W - \omega_B \right) \right] \end{aligned} \tag{36}$$

Results are presented in the following table before the description of identification itself.

parameter	***unit***	***value***
J_B	kgm^2	0.0400
J_W	kgm^2	0.0092
g	$\mathrm{m/s}^2$	9.8067
l	m	0.1090
m_B	kg	1.0000
m_W	kg	1.1000
k_B	N/m	0.4000
k_W	$\mathrm{N/m} \cdot 10^{-5}$	2.1756

Table 4: Identified parameters

The parameters of mass were directly measured with scales. The usual value was used for the gravitational acceleration.

3.1.1.1 Center of Gravity Determination

The single-track robot is hung upside down to the zero operational point and then the whole body is accelerated by an external force. The distance to the center of gravity l is determined from the Christiaan Huygens' law of period of the pendulum (eq. 37), using the small-angle approximation.

$$T = 2\pi \sqrt{\frac{l}{g}} \Rightarrow l = \frac{T^2 g}{4\pi^2} \doteq 10.9\,\mathrm{cm} \tag{37}$$

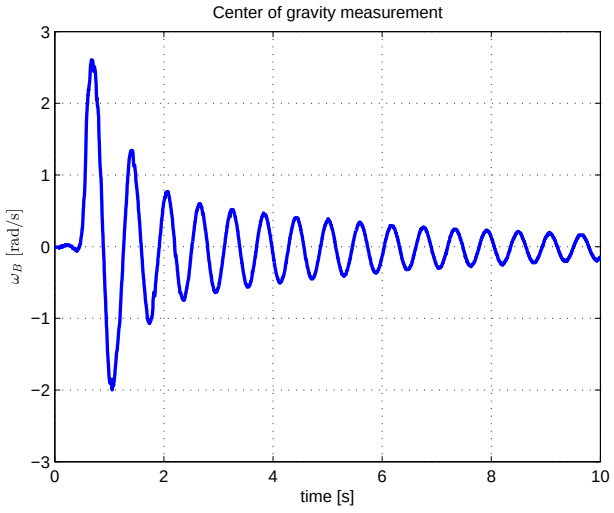

Figure 10: The center of gravity measurement, the body is accelerated by an external force. The value of period is measured and distance to the center of gravity is computed using the Christiaan Huygens' law (eq. 37).

3.1.1.2 Parameters Estimation of ARX

The other parameters are identified by using parameters estimation of the AutoRegresive model with eXternal input (ARX) with the least squares method. The outline of these method's derivation is presented acording to [2]. This method is based on performing N measurements and obtaining N difference equations with up to $2n$ unkown coefficients in the following form

$$\begin{aligned} y(k) &= -a_1 y(k-1) - \ldots - a_n y(k-n) + b_0 u(k) + \ldots + b_n u(k-n) + e(k) \\ y(k+1) &= -a_1 y(k) - \ldots - a_n y(k-n+1) + b_0 u(k+1) + \ldots + b_n u(k-n+1) + e(k+1) \\ &\vdots \\ y(k+N-1) &= -a_1 y(k+N-2) - \ldots - a_n y(k+N-n-1) + \\ &\quad + b_0 u(k+N-1) + \ldots + b_n u(k+N-n-1) + e(k+N-1) \end{aligned} \tag{38}$$

Where e represents the estimation error.

This system of equations is in the terms of matrices formulated as follows.

$$\begin{bmatrix} y(k) \\ y(k+1) \\ \vdots \\ y(k+N-1) \end{bmatrix} = \left[\begin{array}{ccc|cc} -y(k-1) & \ldots & -y(k-n) & u(k) & u(k-n) \\ -y(k) & \ldots & -y(k-n+1) & u(k+1) & u(k-n+1) \\ \vdots & \ldots & \vdots & \vdots & \vdots \\ -y(k+N-2) & \ldots & -y(k+N-n-1) & u(k+N-1) & u(k+N-n-1) \end{array}\right] \begin{bmatrix} a_1 \\ \vdots \\ \frac{a_n}{b_0} \\ \vdots \\ b_n \end{bmatrix} + \begin{bmatrix} e(k) \\ e(k+1) \\ \vdots \\ e(k+N-1 \end{bmatrix} \tag{39}$$

$$\boldsymbol{y} = \boldsymbol{Z\theta} + \boldsymbol{e} \tag{40}$$

The minimization of a quadratic criteria on the estimation error leads to the optimization problem with the following solution including the pseudo inversion.

$$\hat{\boldsymbol{\theta}} = \left(\boldsymbol{Z}^T\boldsymbol{Z}\right)^{-1}\boldsymbol{Z}^T\boldsymbol{y} \tag{41}$$

The initial estimation of the parameters J_B, J_W, k_B, k_W are obtained with this method. The parameters of moments of inertia were further modified by taking the mathematical expression of moment of inertia into consideration. The equation 4 was used for the moment J_B and the moment J_W was modified according to the following equation.

$$J_W = \frac{1}{6} m_W a_W^2$$

Where $a_W = 0.12$m represents the diameter of reaction wheel.

The final simulations which compare the real model with the identified influenced the identification of parameters as well.

3.2 NXT Motor

The NXT Motors with built-in rotation sensor that mesures speed and rotation are used. This type of motors reports the results of measurement to the NXT Intelligent Brick.

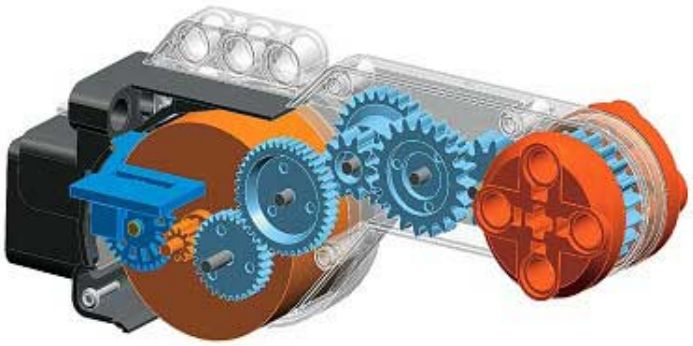

Figure 11: NXT motor, available from [5].

The motor constants are taken from [5, 6] and they are presented in the following table.

constant	unit	description	value
k_e	$\mathrm{V}/_{\mathrm{rad}/\mathrm{s}}$	electric constant	0.4952
R	Ω	resistance	5.2628
L	H	inductance	0.0047
I_{max}	A	maximal curent	0.6000
U_{max}	U	maximal voltage	8.1700

Table 5: NXT motor constants

The input to motors is the voltage, but the output of model is the moment of force. A conversion of the voltage to the moment of force is necessary. Momentum characteristics is presented in the Figure 12a and its derivation is shown in the section 3.2.1.

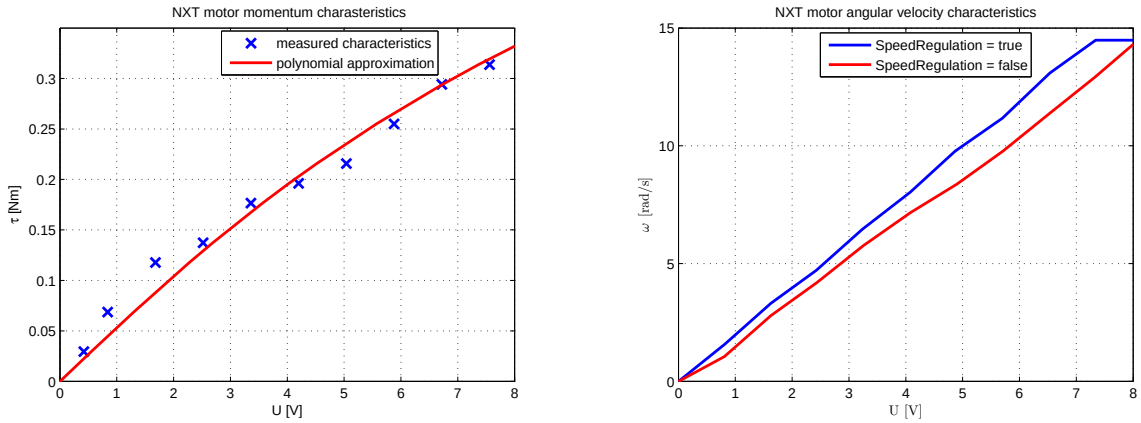

(a) NXT motor momentum characteristics, according to third degree polynomial approximation $U(\tau)$ in least squares sense.

(b) NXT motor angular velocity characteristics with no load describing maximal angular speed ω_W with respect to input voltage U

Figure 12: NXT motor characteristics, relation between moment of force τ and motor input voltage U, angular speed ω_W limitation

The internal implemented speed PID regulator is necessary to be switched off, because the model needs to control the torque instead of the speed reference.

According to the figure 12b a new NXT motor limitation was determined. It is the rotational speed dynamical saturation which is dependent on the input voltage, or input torque. This limitation is possible to be represented by the following relation.

$$\omega_W = 1.7793U - 0.1545 \tag{42}$$

Finding the relation between the quantities U and ω_W the maximal angular velocity is defined with respect to the maximal input voltage presented in the table 5.

$$\omega_{W_{max}} = 14.3824\,\mathrm{rad}/\mathrm{s}$$

3.2.1 Momentum Characteristics

The value of the maximal moment of force was defined as $\tau_{max} \doteq 0.342\,\text{Nm}$ in the Figure 12a. An experiment leading to this characteristics and maximal value is presented in this section.

The special support construction shown in the following picture was made for the NXT Motor.

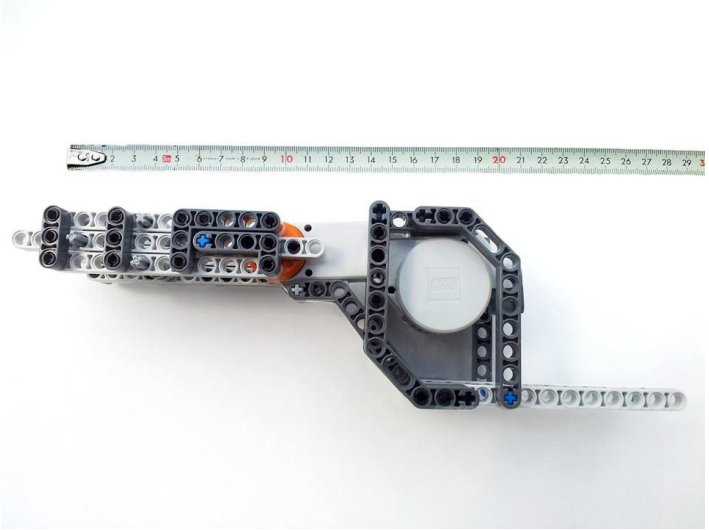

Figure 13: Support construction for the maximal moment of torque measurement.

The experiment is based on the definition of the moment of force.

$$\tau = \|\boldsymbol{r}\|\,\|\boldsymbol{F}\|\sin(\theta)$$

Where $\boldsymbol{r}$ is the vector from the point from which the torque is measured to the point where the force is applied, $\boldsymbol{F}$ is the force vector and θ is the angle between vectors $\boldsymbol{F}$ and $\boldsymbol{r}$. For this experiment, the following is valid $\theta = \frac{\pi}{2} \Rightarrow \sin(\theta) = 1$ and $\|\boldsymbol{r}\| = 0.01\,\text{m}$. The measured quantity is mass and the force $\boldsymbol{F}$, or rather the torque τ is obtained as a product of mass and gravitational acceleration .

The NXT motor with its construction is fixed to the table and the motor pushes in the distance of $\|\boldsymbol{r}\|$ to the digital scale. The final characteristics is shown in the Figure 12a and it's polynomial approximation is determined as

$$U \doteq 48.6606\tau^3 + 18.6752\tau \tag{43}$$

As a comparison according to [1], respectively the equation 1, the relation between the quantities U and τ is defined, neglecting friction forces and the electrical dynamics of the DC-motor.

$$\tau = k_e I = k_u U \Rightarrow U = \frac{\tau}{k_u} \tag{44}$$

$$k_u = \frac{k_e I_{max}}{U_{max}} = 0.0364 \tag{45}$$

This relation is found as inadequate for the NXT motor taking into consideration the measured chracteristics in the Figure 12a.

3.3 Gyroscopic Sensor

HiTechnic NXT Gyro Sensors for the LEGO Mindstorms NXT were used. These sensors detect the rotation, return the number of degrees per second of rotation and indicate the direction of rotation as well. The measuring range is ±360 deg per second. The measurement of angular rotation runs only around one axis.

Figure 14: HiTech NXT Gyro Sensor, availible from [7]. In the left figure sensor design. In the right figure the axis of measurement.

3.3.1 Offset and Drift Corection

Offset error belongs in general to the most frequently occured sensors' error. Each sensor has unique offset value. Gyro sensor was totally motionless during the measurement and the offset value was obtained about 595 $^{\text{deg}}/_{\text{s}}$.

It is necessary to measure not only the angular velocity but the angle too. The angle is obtained by the angular velocity integration, respectively discrete integration. According to this fact the sensor errors influence the angle more than the angular velocity.

The solution to this problem is called the calibration. It consists in the calculation of the anglular velocity average value measured by the gyrocopic sensor e.g. during 5 seconds according to the sample time. Output of the used gyro sensor after the calibration is presented in the figure below.

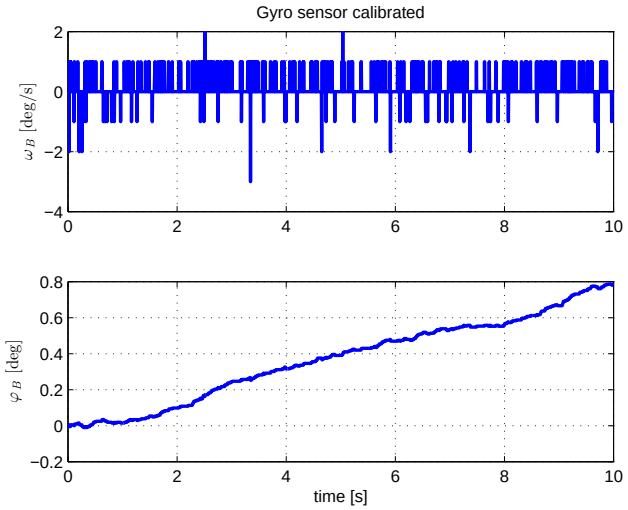

Figure 15: HiTech NXT Gyro Sensor in a motionless state with a calibrated offset error.

It is obvious that the offset value is not constant. This problem is called a sensor drift. A sensor drift is created by several factors, e.g. temperature. The HiTech NXT Gyro Sensors' drift is seriously affected by changes in input voltage. This affection is shown in the following picture, the NXT motor was running during the measurement. This problem is detected also if the NXT battery is powered.

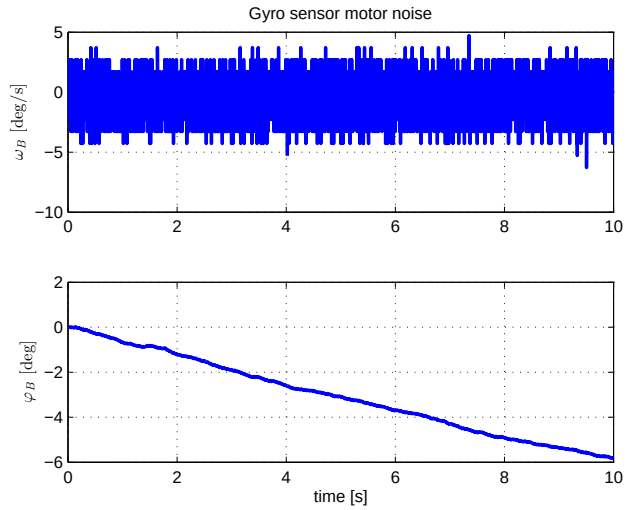

Figure 16: HiTech NXT Gyro Sensor in a motionless state with noise by changes in input voltage.

The technique of constant but slowly updating the value of offset error was used in this project. The high-pass filter was used with following results, the gyro sensor was totally motionless again. This solution deals with the sensor drift very well, but does not solve this problem completely.

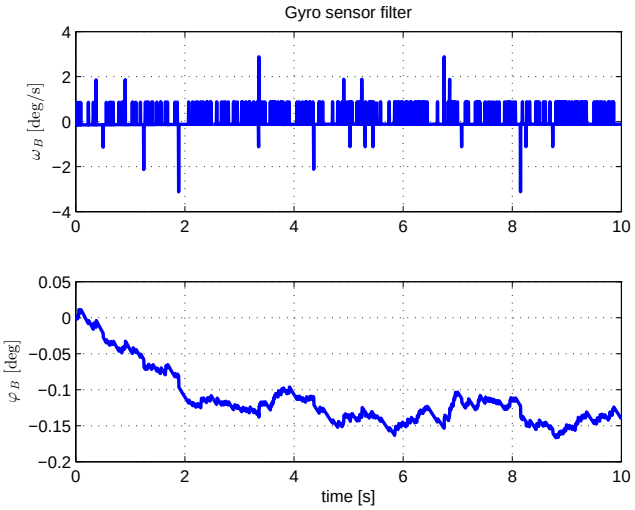

Figure 17: HiTech NXT Gyro Sensor in a motionless state with calibrated offset and filtered drift.

3.4 Final Models Comparison

The final identification test was performed with the single-track robot hung in position upside down in the zero operating point. The reaction wheel was accelerated by random input voltage. The response of the real system, in contrast to the identified which includes all the nonlinearities, is called Identification data fit. It is presented in the following Figure 18.

The identification was succesfully done, as a proof the validation data fit is presented as well. The single-track robot was standing still in the upright position and in the Figure 19 is shown step response which is compared with the identified model. The voltage value of step input is $U = 8\text{V}$.

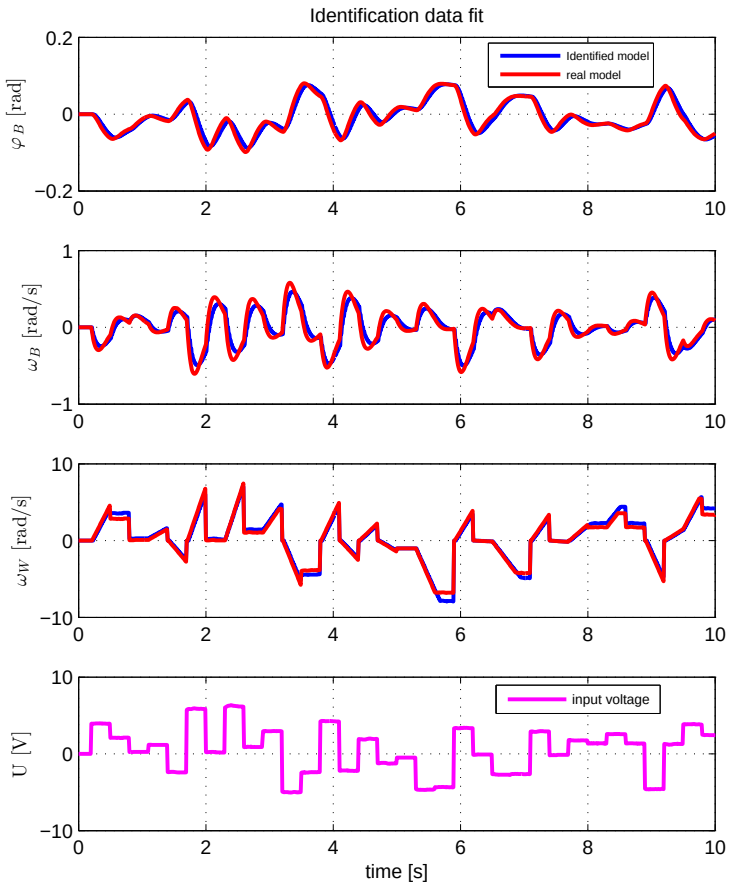

Figure 18: The response of identified and real systems to input voltage. Simulation in position upside down in zero operating point.

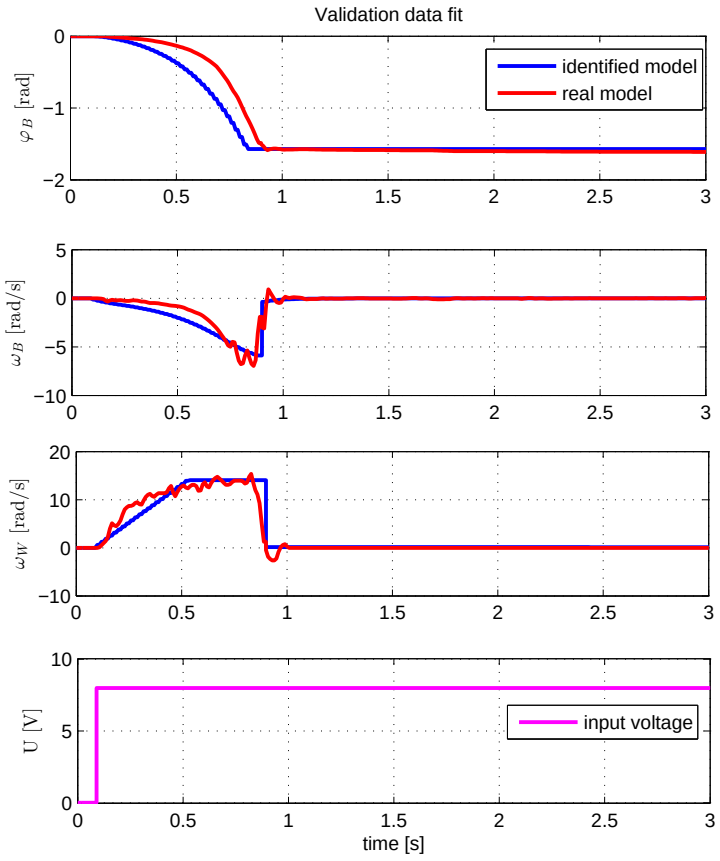

Figure 19: Step response of identified and real systems with the input voltage $U = 8\text{V}$. The single-track mobile robot is placed in the position defined by the angle $\varphi_B = \frac{\pi}{2}\,\text{rad}$ after the falling down. This position means that the robot's body is lying on the ground. The contact between the body and the ground blocks the reaction wheel rotation. According to this fact the reaction wheel is not rotating any more after the collapse. $\left(\frac{\pi}{2}\,\text{rad} = 90\,\text{deg}\right)$

4 Control

4.1 Reaction Wheel Control System Design

By checking the eigenvalues of state matrix $\boldsymbol{A}$ (eq. 18), one unstable pole is found.

The linear continuous-time system is controllable if the controllability matrix (eq.46) is regular, i.e. if it has the full row rank.

$$\boldsymbol{C} = \begin{bmatrix} \boldsymbol{B} & \boldsymbol{AB} & ... & \boldsymbol{A}^{n-2}\boldsymbol{B} & \boldsymbol{A}^{n-1}\boldsymbol{B} \end{bmatrix} \tag{46}$$

where n is the number of states.

The controllability matrix of system (eq. 19) has rank three, there is no problem to control its states using the input moment τ.

4.1.1 Linear Quadratic Regulator Design

For a continuous-time linear system described by state space model with a cost function

$$J = \int_0^\infty \left(\boldsymbol{x}^{\boldsymbol{T}}\boldsymbol{Q}\boldsymbol{x} + u^T\boldsymbol{R}u\right) dt \tag{47}$$

where $\boldsymbol{Q}$ is a diagonal matrix defining the weights of states and $\boldsymbol{R}$ is a matrix defining the weights of inputs, the feedback control law minimizing the cost value is defined as

$$u = -\boldsymbol{K}\boldsymbol{x} \tag{48}$$

The closed loop system, in which only the state matrix $\boldsymbol{A}$ is changed as follows, is defined after the calculations, finding values of matrix $\boldsymbol{K}$ and application of the feedback.

$$\boldsymbol{A_C} = (\boldsymbol{A} - \boldsymbol{BK}) \tag{49}$$

The important stability condition is satisfied by this closed loop system.

$$eig\,(\boldsymbol{A_C}) \leqq 0 \tag{50}$$

The functionality of designed LQR is shown in the Figure 20.

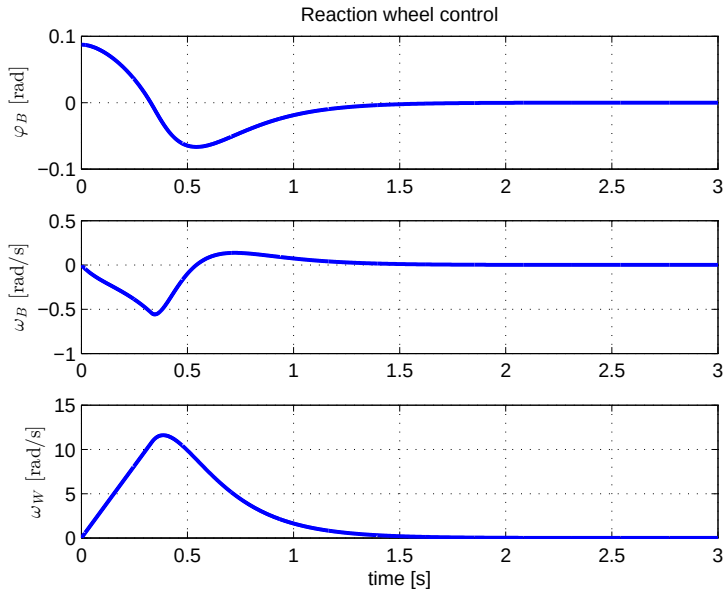

Figure 20: The reaction wheel pendulum controlled by the linear quadratic regulator. Initial conditions: $\boldsymbol{x_0} = \begin{bmatrix} 0.0873 & 0 & 0 \end{bmatrix}^T$. ($0.0873\,\text{rad} \doteq 5\,\text{deg}$)

4.2 Gyroscopic Control System Design

One unstable pole and one pole in zero are determined, but the row rank of controllability matrix $\boldsymbol{C}$ is full. The linear quadratic regulator with ω_G as the control input and φ_B as the control output is used again.

4.2.1 Linear Quadratic Regulator Design

By applying the control law (eq. 48) and changing the state matrix $\boldsymbol{A}$ (eq. 49), the closed loop system with all stable poles is derived. The simulations of designed LQR are shown in the following figure.

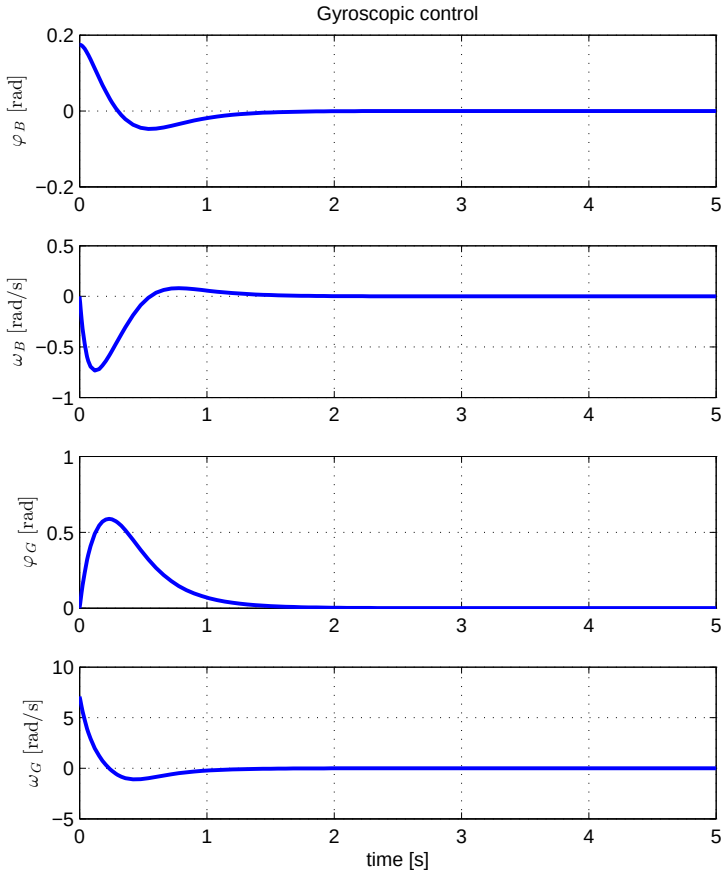

Figure 21: Gyroscopic control with the LQR. Initial conditions: $\boldsymbol{x_0} = \begin{bmatrix} 0.1745 & 0 & 0 \end{bmatrix}^T$. The angle of the robot´s body is φ_B, the angular velocity of the body is ω_B, the gyroscopic disc angle of rotation is φ_G and ω_G is its angular velocity. ($0.1745\,\text{rad} \doteq 10\,\text{deg}$)

4.3 Control Design of Planar Model of Motion

One unstable pole and one pole in zero were found by calculating the eigenvalues of matrix $\boldsymbol{A}$ (eq. 33). The controllability matrix $\boldsymbol{C}$ has full rank, no uncontrollable state exists. Only the input τ is used as the control input, α and $\dot{\alpha}$ are uncontrollable inputs.

4.3.1 Linear Quadratic Regulator Design

Applying the same control law as in the sections before the new stable system is derived. The simulation of the designed LQR is shown in the Figure 22a.

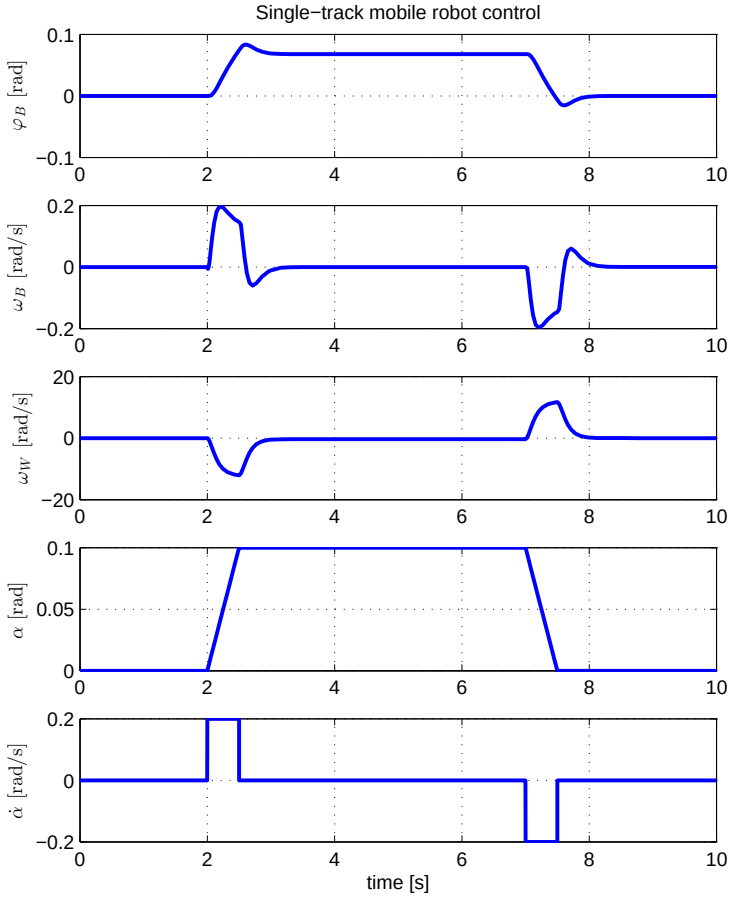

(a) Single-track mobile robot planar model of motion with the constant speed $v = 1\,\mathrm{m/s}$. The quantities φ_B, ω_B, ω_W desribe the reaction wheel control and α, $\dot{\alpha}$ desribe the rotation of the front wheel. Simulation represents the rotation of the front wheel about the angle $\alpha = 0.1\,\mathrm{rad}$ and following straightening the direction of motion. $\left(0.1\,\mathrm{rad} \doteq 6\,\mathrm{deg}\right)$

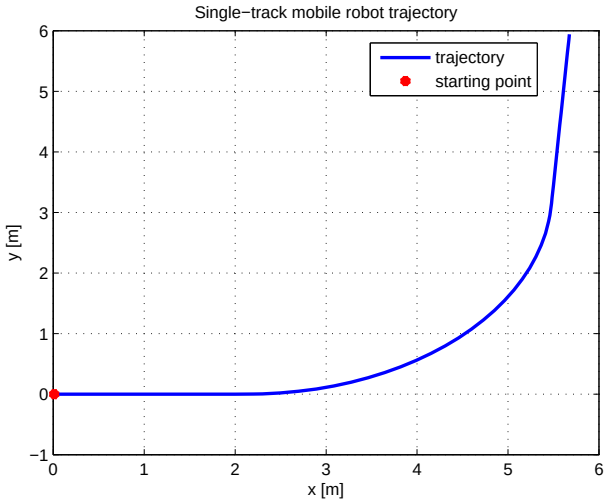

(b) Single-track mobile robot trajectory corresponding to 22a

Figure 22: Single-track mobile robot LQR control with the graphs of important variables and demonstration of the robot's trajectory.

4.4 Real Control System Design

The final section deals with the real model control. The linear quadratic regulator was applied according to the section 4.1.1. Using the Matlab environment the LQR design is reduced only to the design of the weight matrices $\boldsymbol{Q}$, $\boldsymbol{R}$. The final quantified state matrices $\boldsymbol{A}$, $\boldsymbol{B}$ are defined as

$$\boldsymbol{A} = \begin{bmatrix} -10.0005 & 56.1377 & 0.0005 \\ 1.0000 & 0 & 0 \\ 0.0024 & 0 & -0.0024 \end{bmatrix} \boldsymbol{B} = \begin{bmatrix} -25.0000 \\ 0 \\ 108.6957 \end{bmatrix} \tag{51}$$

where system with these state matrices (eq. 51) is unstable because of one positive pole $p_2 = 4.0075$. The privileged states are φ_B and ω_W, according to this fact the matrix of state weights $\boldsymbol{Q}$ is determined. The requirements to an input are given by selecting the significantly greater value of input weight in the matrix $\boldsymbol{R}$.

After using the Matlab to solve the optimization problem of minimizing the cost function J (eq. 47) the discrete linear quadratic regulator is calculated according to the equation 48 and the closed loop matrix $\boldsymbol{A_C}$ (eq. 49) is determined.

$$\boldsymbol{A_C} = \begin{bmatrix} -17.7110 & -51.8715 & -0.0005 \\ 1.0000 & 0 & 0 \\ 33.5263 & 469.6055 & 0.0022 \end{bmatrix} \tag{52}$$

where the eigenvalues which fulfill the condition (eq. 50) are

$$\begin{aligned} \lambda_1 &= -14.0081 \\ \lambda_2 &= -3.6984 \\ \lambda_3 &= -0.0024 \end{aligned}$$

The maximal controllable value of the robot vertical angle displacement $\varphi_B = 0.1222\,\text{rad} \doteq 7\,\text{deg}$ was also found. It was estimated using the closed loop model (eq. 52) identified in the section 3which includes the input saturation limit $\tau_{sat} = \pm 0.342\,\text{Nm}$.

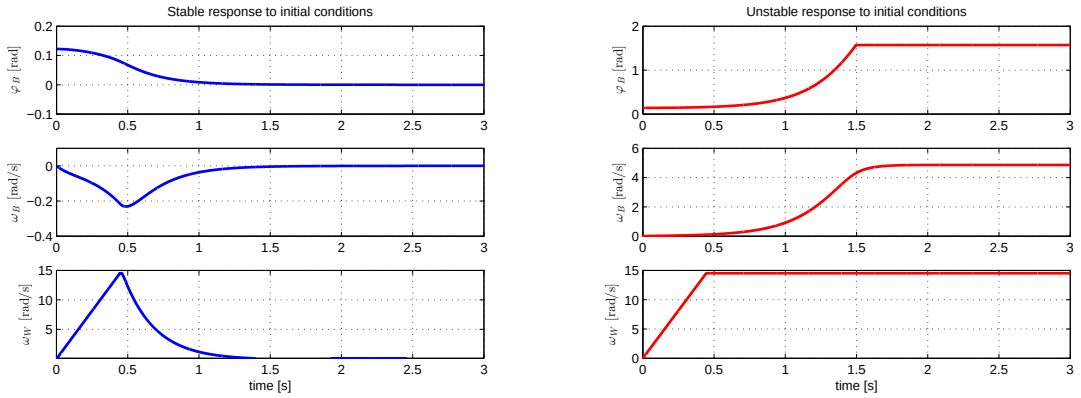

(a) Initial conditions: $\boldsymbol{x_0} = [0.1222\,0\,0]$. Stable response. $\left(0.1222\,\text{rad} \doteq 7\,\text{deg}\right)$

(b) Initial conditions: $\boldsymbol{x_0} = [0.1369\,0\,0]$. Cannot be straightened, unstable. $\left(0.1369\,\text{rad} \doteq 8\,\text{deg}\right)$

Figure 23: Identified model response of the single-track robot with the reaction wheel to inicial conditions.

Finally, the LEGO Mindstorms brick brings a lot of limitations. The gyroscopic drift problem turned out as the crucial disadvatage which obstructs the lateral stabilization despite the filtration. The high-pass filter solves the drift error relatively well but not completely. The single-track mobile robot loses it´s zero reference point very quickly and then the keeping in the upright position is unattainable. Getting the angle value of φ_B by the integration of measured value ω_B increases the influence of drift significantly. Due to this failure few real data measurements are presented in this section.

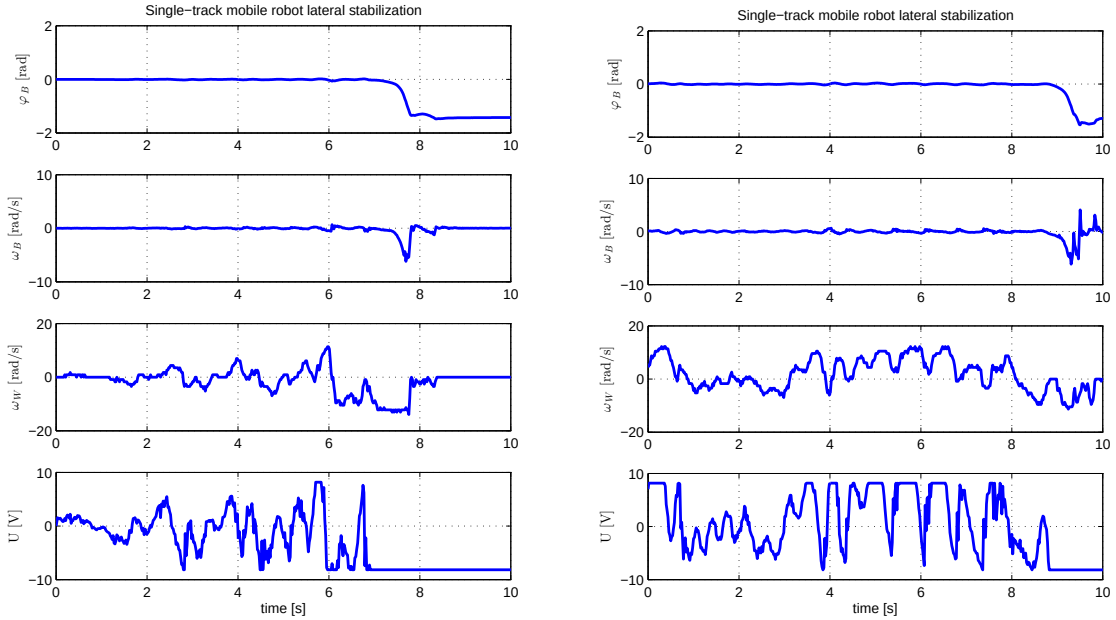

Figure 24: Single-track mobile robot lateral stabilization, real data measurement using MATLAB environment with RWTH Mindstorms NXT toolbox [19]

The selfbalancing motorbike destabilizes itself during the stabilization effort. It is shown in the Figure 24. The robot exceeds the maximal controllable angle of body φ_B and the input voltage U reaches the saturation limit. The reaction wheel cannot rotate any more when the robot's body falls to the ground. The contact between the body and the ground blocks the reaction wheel rotation. According to this fact the behavior of the angular velocity ω_W is obvious in the Figure 24.

5 Conclusion

The mathematical models presented in the section 2 were succesfully determined by the attractive results including the simulations of their control (Fig. 20, 21, 22). This theoretical part of the thesis is worked out satisfactory and an output of this part is an evaluation of how feasible it is to design the real model with a help of the LEGO Mindstorms building kit. It was decided according to the theoretical results that the gyroscopic control is the most attractive method of single-track mobile robot lateral stabilization, but the realization is very difficult from the design and material point of view. It is presented in [18] that a gyroscopic control realization looks very impressive with sufficient resources. The behaviour of a motorbike which is stabilized by the gyroscopes is very safe and reliable and can resist to the various attempts of displacement. However, the building kit chosen for this thesis does not provide the components to realize this method of control.

The reaction wheel control was chosen as the most appropriate method for the realization with a help of the LEGO Mindstorms, but a lot of both expected and unexpected limitations were occured during the identification (sec. 3). All these limitations are presented. They contain primarily the gyro sensor drift, the maximal battery voltage or the limitations of NXT motor. The gyro sensor drift significantly shifts the zero position of the single-track mobile robot despite a filtering and this fact makes the vertically upright position difficult to control. Maximal NXT brick sample time is worth mentioning as it is quite slow according to the computational complexity. A new version of LEGO Mindstorms is called the EV3 [20] and its sample rate is a little bit better. The real model was constructed in spite of all these disadvantages and sufficiently demonstrates the principles of reaction wheel control.

The control is discussed and described in the last section 4. The controlled real model behaviour is expected but unsatisfactory. Some quite interesting balancing measurements are presented in this section. However, unfortunately this model cannot be seen as a reliable selfbalancing motorbike. The designed control is not sufficient, probably because of some not included nonlinearities. It is shown in the presented tests that the robot destabilizes itself during the stabilization effort. This effect was not solved by the LQR tunning.

The sensor's drift minimization along with a method other than the high-pass filter could make the lateral stabilization significantly better and more reliable. However, the NXT motor torque saturation is finally determined as the biggest disadvantage. The maximal controlable angle of vertical displacement which was defined as $\varphi_B = 7°$ could be increased using the suitable type of DC-motor with sufficient torque. These motors are unfortunately not offered by the LEGO manufacturer. Due to this fact the DC-motor from an external source is recommended. Finally, one more improvement proposal is possible, it is specifically increasing the reaction wheel weight. This weight was not increased in the presented real model because the model strenght would be disrupted. However, the lateral stabilization success is not guaranteed by taking into consideration all these improvement proposals. An effort to design the LQR which would fulfill all the requirements will continue.

References

[1] Block, D. J., Åström,K.J. and Spong M.W. (2007): 'Reaction wheel pendulum', San Rafael, Calif : Morgan, 2007 ISBN 15-982-9194-7

[2] Roubal, J. a Hušek, P. (2011): 'Regulační technika v příkladech', 1. vyd. Prague: BEN - technická literatura, 2011 ISBN 978-80-7300-260-2

[3] Franklin, G. F. (2006): 'Feedback control of dynamic systems', 5th ed. Upper Saddle River: Pearson Education, 2006, xxii, 276, ii s ISBN 01-314-9930-0

[4] Turner, G.: Gyroscopes [online] [cit 2014-05-17] Availible from WWW: (http://www.gyroscopes.org)

[5] Hurbain, P.: Philo's Home Page [online] [cit 2014-05-17] Availible from WWW: (http://philohome com/)

[6] Maxim,: NXT Lego Mindstorms Programming [online] [cit 2014-05-17] Availible from WWW: (http://nxt-unroller.blogspot.cz/2011/01/motor-controller-with-feed-forward-for.html)

[7] HiTechnic Products, [online] [cit 2014-05-17] Available from WWW: (http://www.hitechnic.com/cgi-bin/commerce.cgi?preadd=action&key=NGY1044)

[8] NXT Time, [online] [cit 2014-05-17] Availible from WWW: (http://nxttime.wordpress.com/tag/gyro-sensor/)

[9] Biswas, J., Seth, B. (2008): 'Dynamic stabilisation of a reaction-wheel actuated wheel-robot' , International Journal of Factory Automation, Robotics and Soft Computing, Issue 4, Published by INTERNATIONALSAR, October 2008, p.96-101, ISSN 1828-6984.

[10] Spong, W.M., Corke, P., Lozano, R. (2001): 'Nonlinear control of the reaction wheel pendulum', Automatica, 37(2001), s. 1845.

[11] Seman, P.,Juhás, M. (2011): 'Swing up ans stadilization of reaction wheel pendulum' in The 4th International conference Modelling of Mechanical and Mechatronic systems 2011, September 20 – 22, 2011 Herľany, Slovak Republic

[12] Andrievsky, B.R. (2011): 'Global stabilization of the unstable reaction-wheel pendulum', Automation and Remote Control, 72(9), pp. 1981-1993.

[13] Jepsen, F., Anders, S., Anders, R.P., Zhenyu, Y. (2009): 'Development and control of an inverted pendulum driven by a reaction wheel' in International Conference on Mechatronics and Automation August 9 - 12, Changchun, China

[14] Beznos, A.V., Formalsky, A.M., Gurfinkel, E.V., Jicharev, D.N., Lensky, A.V., Savitsky, K.V., Tchesalin L.S. (1998):'Control of autonomous motion of two- wheel bicycle with gyroscopic stabilisation' in International Conference on Robotics and Automation , 1998, Leuven, Belgium, pp. 2670-2675

[15] Guo, L., Liao, Q., Wei, S., Zhuang, Y. (2009): 'Design of Linear Quadratic Optimal Controller for Bicycle Robot' in International Conference on Automation and Logistics (ICAL), August, 2009, Shenyang, China, pp. 1968-1972

[16] PendCon, [online] [cit 2014-05-17] Availible from WWW: (http://www.pendcon.de/Reaction_Wheel_Pendulum.html)

[17] Davol, A., Owen, F.,:'Dynamic model of a bicycle from kinematic and kinetic considerations', California Polytechnic State University, San Luis Obispo, California

[18] LitMotors [online] [cit 2014-05-17] Available from WWW: (http://litmotors.com/c1/)

[19] Lehrstuhl für Bilderarbeitung:'RWTH-Mindstorms NXT toolbox' [online] [cit 2014-05-17] Availible from WWW:(http://www.mindstorms.rwth-aachen.de/)

[20] LEGO.com Mindstorms [online] [cit 2014-05-17] Availible from WWW: (mindstorms.lego.com/)

A Gyroscopic Effect

First step to define the system controlled by a gyroeffect is to derive the physical principle of the gyroscopic effect. This derivation is based on a rotation of a continuous body around an axis. Because of the easier notation the bold marking of the time variables is used here in the contrast with the previous sections.. The angular momentum of continuous body is defined as

$$\boldsymbol{L} = \int \boldsymbol{r} \times (\boldsymbol{\omega} \times \boldsymbol{r})\, dm \tag{53}$$

The vectors can be divided into three basic axis.

$$\begin{aligned} \boldsymbol{L} &= L_x\boldsymbol{i} + L_y\boldsymbol{j} + L_z\boldsymbol{k} \\ \boldsymbol{r} &= r_x\boldsymbol{i} + r_y\boldsymbol{j} + r_z\boldsymbol{k} \\ \boldsymbol{\omega} &= \omega_x\boldsymbol{i} + \omega_y\boldsymbol{j} + \omega_z\boldsymbol{k} \end{aligned} \tag{54}$$

Applying the equations 54 to the equation 53

$$\begin{aligned} \boldsymbol{L} = & \left[\omega_x \int (y^2+z^2)dm - \omega_y \int (xy)dm - \omega_z \int (xz)dm\right]\boldsymbol{i} + \\ & + \left[-\omega_x \int (xy)dm + \omega_y \int (x^2+z^2)dm - \omega_z \int (yz)dm\right]\boldsymbol{j} + \\ & + \left[-\omega_x \int (zx)dm - \omega_y \int (yz)dm + \omega_z \int (x^2+y^2)dm\right]\boldsymbol{k} \end{aligned} \tag{55}$$

The moment of inertia and the product of inertia are now important to be defined and applied to the equation 55.

$$\begin{aligned} J_x &= \int \left(y^2+z^2\right) dm \\ J_y &= \int \left(x^2+z^2\right) dm \\ J_z &= \int \left(x^2+y^2\right) dm \\ D_{xy} &= \int (xy)\, dm \\ D_{xz} &= \int (xz)\, dm \\ D_{yz} &= \int (yz)\, dm \end{aligned}$$

$$\boldsymbol{L} = \omega_x J_x - \omega_y D_{xy} - \omega_z D_{xz} - \omega_x D_{xy} + \omega_y J_y + \omega_z D_{yz} - \omega_x D_{xz} - \omega_y D_{yz} + \omega_z J_z$$

It is defined, that the body is in the origin of coordinate system and that the rotation axis pass through the origin. According to this fact they are called principal axes of inertia, all the products of inertia are equal to zero and the angular momentum is defined as

$$\boldsymbol{L} = L_x\boldsymbol{i} + L_y\boldsymbol{j} + L_z\boldsymbol{k} = \omega_x J_x\boldsymbol{i} + \omega_y J_y\boldsymbol{j} + \omega_z J_z\boldsymbol{k} \tag{56}$$

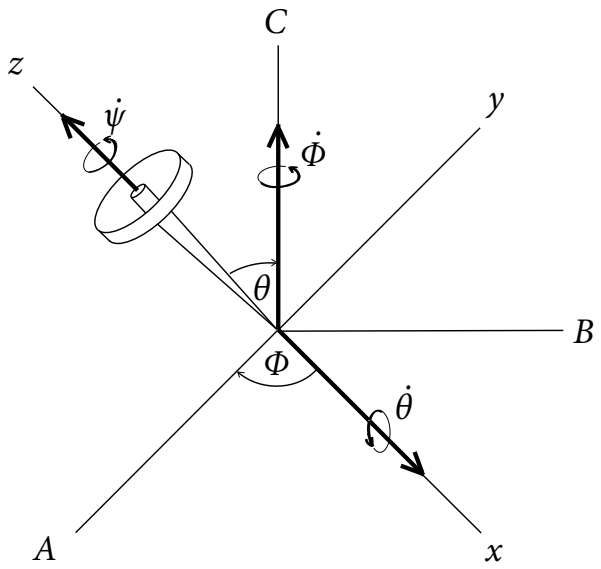

Figure 25: Gyroscopic effect scheme with reference ABC axes and angles with angular rotations definition θ, ϕ, ψ, $\dot{\boldsymbol{\theta}}$, $\dot{\boldsymbol{\phi}}$, $\dot{\boldsymbol{\psi}}$

There are two systems shown in the Figure 25. The first is a rotation coordinate system with origin at the pivot point of the gyro (xyz axes) which fulfills the condition of neglecting all the products of inertia because they equal zero. The second is a fixed coordinate system which serves as a reference (ABC axes).

$$\begin{aligned} \dot{\boldsymbol{\theta}} &= \textit{nutation} \\ \dot{\boldsymbol{\phi}} &= \textit{precession} \\ \dot{\boldsymbol{\psi}} &= \textit{spin} \end{aligned}$$

The rotation coordinate system follows only the gyroscopic nutation and precession. The angular velocity of the rotation coordinate system xyz is given by

$$\boldsymbol{\Omega} = \dot{\boldsymbol{\theta}} + \dot{\boldsymbol{\phi}}$$

The angular velocity of gyro with respect to the fixed coordinate system ABC is given by

$$\boldsymbol{\omega} = \dot{\boldsymbol{\theta}} + \dot{\boldsymbol{\phi}} + \dot{\boldsymbol{\psi}}$$

The Euler angles θ, ϕ, ψ define the displacement of gyro with respect to the fixed coordinate system ABC.

The total moment of force supplied by gyro in each axis x, y, z is formulated.

$$
\begin{aligned}
\boldsymbol{\tau} &= \frac{d\boldsymbol{L}}{dt} \\
\left(\frac{d\boldsymbol{L}}{dt}\right)_{ABC} &= \dot{L}_x\boldsymbol{i} + \dot{L}_y\boldsymbol{j} + \dot{L}_z\boldsymbol{k} + L_x\dot{\boldsymbol{i}} + L_y\dot{\boldsymbol{j}} + L_z\dot{\boldsymbol{k}} = \dot{L}_x\boldsymbol{i} + \dot{L}_y\boldsymbol{j} + \dot{L}_z\boldsymbol{k} + \boldsymbol{\Omega}\times\boldsymbol{L} \\
\boldsymbol{\tau} &= \dot{L}_x\boldsymbol{i} + \dot{L}_y\boldsymbol{j} + \dot{L}_z\boldsymbol{k} + \boldsymbol{\Omega}\times\boldsymbol{L}
\end{aligned}
$$

According to the equation 56

$$
\boldsymbol{\tau} = J_x\dot{\omega}_x\boldsymbol{i} + J_y\dot{\omega}_y\boldsymbol{j} + J_z\dot{\omega}_z\boldsymbol{k} + [(\Omega_x\boldsymbol{i} + \Omega_y\boldsymbol{j} + \Omega_z\boldsymbol{k}) \times (J_x\omega_x\boldsymbol{i} + J_y\omega_y\boldsymbol{j} + J_z\omega_z\boldsymbol{k})] \tag{57}
$$

where

$$
\begin{aligned}
J_x &= J_x + mR^2 \\
J_y &= J_y + mR^2 \\
J_z &= J_z
\end{aligned}
$$

For each axis individually

$$
\begin{aligned}
\tau_x &= J_x\dot{\omega}_x - J_y\Omega_z\omega_y + J_z\Omega_y\omega_z \\
\tau_y &= J_y\dot{\omega}_y - J_z\Omega_x\omega_z + J_x\Omega_z\omega_x \\
\tau_z &= J_z\dot{\omega}_z - J_x\Omega_y\omega_x + J_y\Omega_x\omega_y
\end{aligned} \tag{58}
$$

The angular velocities $\boldsymbol{\Omega}$ and $\boldsymbol{\omega}$ could be rewritten as follows.

$$
\begin{aligned}
\boldsymbol{\Omega} &= \dot{\boldsymbol{\theta}} + \dot{\boldsymbol{\phi}} \\
\boldsymbol{\Omega} &= \Omega_x\boldsymbol{i} + \Omega_y\boldsymbol{j} + \Omega_z\boldsymbol{k} \\
\boldsymbol{\Omega} &= \dot{\theta}\boldsymbol{i} + \dot{\phi}\sin(\theta)\,\boldsymbol{j} + \dot{\phi}\cos(\theta)\,\boldsymbol{k}
\end{aligned} \tag{59}
$$

$$
\begin{aligned}
\boldsymbol{\omega} &= \dot{\boldsymbol{\theta}} + \dot{\boldsymbol{\phi}} + \dot{\boldsymbol{\psi}} \\
\boldsymbol{\omega} &= \omega_x\boldsymbol{i} + \omega_y\boldsymbol{j} + \omega_z\boldsymbol{k} \\
\boldsymbol{\omega} &= \dot{\theta}\boldsymbol{i} + \dot{\phi}\sin(\theta)\,\boldsymbol{j} + \left(\dot{\phi}\cos(\theta) + \dot{\psi}\right)\boldsymbol{k}
\end{aligned} \tag{60}
$$

Substituing the relations (eq. 59, 60) into the equations 58 it is obtained

$$
\begin{aligned}
\tau_x &= J_x\ddot{\theta} - J_y\dot{\phi}^2\cos(\theta)\sin(\theta) + J_z\dot{\phi}\sin(\theta)\left(\dot{\phi}\cos(\theta) + \dot{\psi}\right) \\
\tau_y &= J_y\left(\ddot{\phi}\sin(\theta) + \dot{\phi}\dot{\theta}\cos(\theta)\right) - J_z\dot{\theta}\left(\dot{\phi}\cos(\theta) + \dot{\psi}\right) + J_x\dot{\phi}\dot{\theta}\cos(\theta) \\
\tau_z &= J_z\left(\ddot{\phi}\cos(\theta) - \dot{\phi}\dot{\theta}\sin(\theta) + \ddot{\psi}\right) - J_x\dot{\phi}\dot{\theta}\sin(\theta) + J_y\dot{\theta}\dot{\phi}\sin(\theta)
\end{aligned} \tag{61}
$$

In one specific case, where the precession and spin are constant and nutation angle equals to 90° as shown in the Figure 26.

$$\begin{aligned} \dot{\theta} &= 0 \\ \ddot{\phi} &= 0 \\ \ddot{\psi} &= 0 \end{aligned}$$

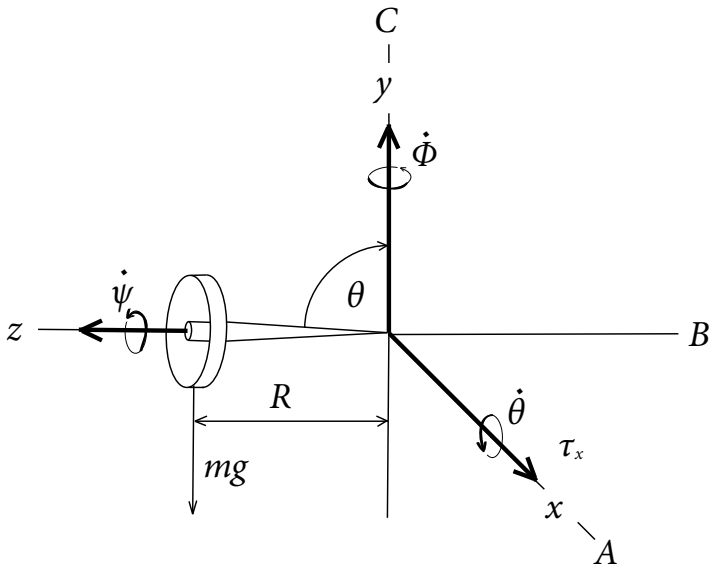

Figure 26: Specific case of gyroscopic position with nutation $\theta = 90°$

Then the solution becomes very easy.

$$\begin{aligned} \tau_x &= J_z \dot{\phi} \dot{\psi} \\ \tau_x &= mgR \end{aligned} \tag{62}$$

The moment of inertia for a solid circular disk is defined as

$$J_z = \frac{1}{2} m r^2$$

For a thin circular ring

$$J_z = m r^2$$

where r is the radius of the disk or the ring.

The final moment of force, which is necessary to single-track mobile robot control, is derived.

$$\tau_x = \frac{1}{2} m r^2 \dot{\phi} \dot{\psi} \tag{63}$$

B Contents of The CD Attached

1. Electronic Version of This Thesis (**BAP.pdf**)
2. Reaction Wheel MATLAB Model (**reactWheelModel.slx**)
3. Reaction Wheel MATLAB Script (**reactWheelScript.m**)
4. Gyroscopic Control MATLAB Model (**gyroModel.slx**)
5. Gyroscopic Control MATLAB Script (**gyroScript.m**)
6. Planar Model of Motion MATLAB Model (**motionModel.slx**)
7. Planar Model of Motion MATLAB Script (**motionScript.m**)
8. Identified MATLAB Model (**identifiedModel.slx**)
9. Identified MATLAB Script (**identifiedScript.m**)
10. LEGO Mindstorms Control MATLAB Script (**legoControl.m**)